IEEE Access
Multidisciplinary | Rapid Review | Open Access Journal

Received March 30, 2021, accepted April 12, 2021, date of publication April 19, 2021, date of current version April 28, 2021.

Digital Object Identifier 10.1109/ACCESS.2021.3073958

MEMS Sensors for Diagnostics and Treatment in the Fight Against COVID-19 and Other Pandemics

MUHAMMAD SHAHBAZ KHAN, MUHAMMAD OWAIS TARIQ, MENAA NAWAZ, AND JAMEEL AHMED, (Member, IEEE)
Department of Electrical Engineering, Riphah International University, Islamabad 44000, Pakistan
Corresponding author: Muhammad Shahbaz Khan (engr.msk90@gmail.com, 3197@students.riu.edu.pk)

ABSTRACT As the world is going through an existential global health crisis, i.e., the outbreak of novel coronavirus-caused respiratory disease (Covid-19), the healthcare systems of all the countries require readily available, low cost and highly precise equipment for the rapid diagnostics, monitoring, and treatment of the disease. The performance and precision of this equipment are solely dependent on the sensors being used. The advancement in research and development of micro-electro-mechanical systems (MEMS) based sensors during recent years, has resulted in the improvement of the conventional equipment being used in biomedical and health care applications. Microfluidics (Lab-on-a-chip) and MEMS sensors are now being used extensively for quick and accurate detection, progression monitoring, and treatment of various diseases including Covid-19. The ongoing miniaturization and design improvements have resulted in more precise sensors and actuators for healthcare applications, even for micro and nanoscale measurements in drug delivery and other invasive applications. This article aims at reviewing the MEMS sensors being used or which can be used in the important equipment for the detection and treatment of Covid-19 or other pandemics. An insight into various designs and working principles of the research-based and commercially available MEMS sensors is presented. The study highlights the role and importance of MEMS sensors in the improvement of equipment with conventional sensors. MEMS sensors outperform the conventional sensors due to their small size (1μm-1mm), negligible weight, prompt response, precise measurements, portability, and ease of integration with electronic circuitry.

INDEX TERMS COVID-19, MEMS, MEMS sensors, SARS-CoV-2.

I. INTRODUCTION

With every passing day, the number of covid-19 patients has been increasing since the outbreak. The outbreak started in mid-December of 2019 [1] and has taken the world by storm since then. More than 185 countries and territories have been reported to get infected by the deadly virus up till now. The situation escalated after December 2019, when the World Health Organization (WHO) reported multiple cases of pneumonia of an unknown etiology in Wuhan, the city of Hubei Province in China, by their health authorities. On January 8, 2020, the Chinese Center for Disease Control and Prevention took only a few days to officially announce it as a novel coronavirus that is the causative pathogen of COVID-19 [2]. By the end of January 2020, the WHO announced this outbreak as a public health emergency around the globe [3]. As of 7 March 2021, nearly 118 million confirmed cases of COVID-19 and 2.62 million deaths have been reported globally [4]. The number of COVID-19 cases reported weekly by WHO regions, and global deaths, as of 7 March 2021 is shown in Fig. 1. The number of confirmed cases might be lower than the number of actual cases due to limited testing worldwide.

After the outbreak, numerous researchers around the world started pouring investigations and results about the novel virus. This virus comes from a family of viruses that can be categorized into two groups, i.e., alpha coronavirus and beta coronavirus, often causing normal cold with upper respiratory tract infections in the human body [5].

Severe acute respiratory syndrome (SARS) is a type of coronavirus which was first identified in 2003 but the first human infection took place in November 2002. The SARS epidemic started in November 2002 and ended in July 2003 compromising the health of more than 8000 people with 774 deaths in 29 territories [5]. As far as MERS is concerned, it started in 2012 in Saudi Arabia [6], and up till now, around 2500 cases have been reported with 866 deaths reaching

The associate editor coordinating the review of this manuscript and approving it for publication was Michail Kiziroglou.

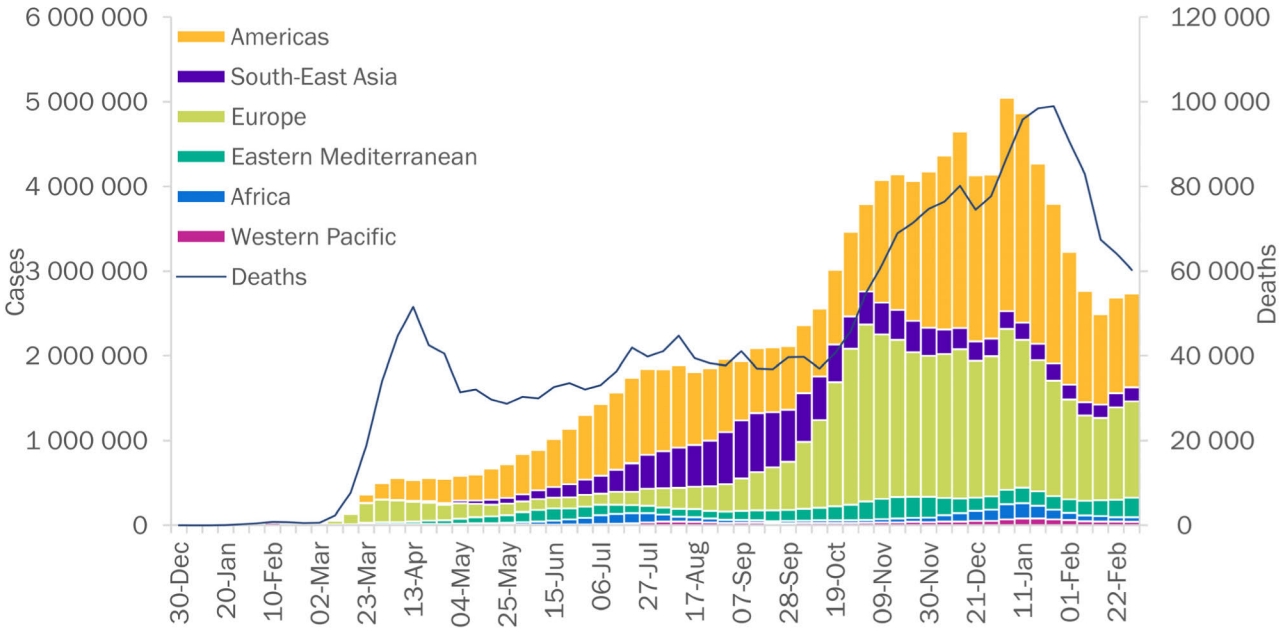

FIGURE 1. The number of COVID-19 cases reported weekly by WHO regions, and global deaths, as of 7 March 2021 [4].

to 34.3% fatality rate [7]. MERS-CoV causes pulmonary failure due to acute lung injury (ALI) and acute respiratory distress syndrome (ARDS), which often results in death. The International Committee on Taxonomy of Viruses named the current novel virus as SARS-CoV-2 and the disease is termed COVID-19 [8]–[10].

A. SPREAD TRENDS

The health authorities in China were alerted in December 2019, when most of the reported cases originated from the Huanan wholesale seafood local market [11]. Sars-CoV-2 has been found to be more likely infectious for people with underlying chronic comorbidities including cardiovascular, cerebrovascular diseases, and diabetes as well [12]. The highest proportion of severe cases have been found to be occurring in adults with ages more than 50 years and those with certain underlying conditions as mentioned above [13]. Furthermore, human to human transmission has proved it to be extremely contagious.

B. TRANSMISSION

SARS-CoV-2 is categorized as one of the novel Betacoronavirus infecting humans. It has been found that the SARS-CoV-2 is quite similar to (88% identity) two other coronaviruses, which were also discovered in China in 2018 (bat-SL-CoVZC45 and bat-SL-CoVZXC21) [14]. These studies have suggested that all these viruses might have derived from bats which led to the possibility of human-to-human transmission later [14]–[16]. The source of contact during human transmission might include the respiratory droplets of an infected person; they could reach anyone who is in close contact with an infected person through coughs or sneezes. The other person could inhale those droplets via mouth or nose and the virus can enter the body. Various studies have also shown asymptomatic transmission in many cases as well [17]. It has also been confirmed that SARS-CoV-2 has a higher transmission rate in comparison to SARS-CoV. Furthermore, hospital-related transmission in new patients is suspected to be 41% [13].

C. FATALITY RATE

The mortality rate for confirmed Covid-19 cases, issued by the National Health Commission of China, was 2.1% as of February 4, 2020 [18] whereas from the rest of the world, it was reported as 0.2% on that date [19]. A significant decrease (20-30%) in lung capacity has also been observed in some recovered cases due to irreversible fibrosis as a result of the virus [20]. This is a medical condition where lung tissue is scarred and stiffened, causing severe and permanent damage to the lungs. The damage might lead to severe respiratory issues such as acute respiratory distress syndrome (ARDS) in ∼22.5% of cases and can affect the immune system as well [21]. Currently, the global death rate as of 7 March 2021 is 2.22% globally, as there have been nearly 118 million reported confirmed cases including 2.62 million reported deaths [4].

D. SYMPTOMS

The symptoms of SARS and COVID-19 can be categorized as systematic and respiratory disorders as shown in Table 1. Systematic disorders include fever with dry cough and a lot of fatigue, whereas the major respiratory disorders comprise rhinorrhea, sneezing, sore throat, and pneumonia.

Other symptoms as observed in the hematology can include lower platelet count, Leukopenia, and lymphopenia [22], [23]. However, respiratory symptoms are more

TABLE 1. Comparison of SARS and Covid-19.

Disorder	SARS	COVID-19
Systematic Disorders	High fever Headache Dry cough Fatigue Diarrhea	Fever Headache Cough Fatigue Diarrhea Sputum production Hemoptysis Dyspnea Lymphopenia
Respiratory Disorders	Rhinorrhea Sneezing Sore throat Pneumonia Mild respiratory problem	Rhinorrhea Sneezing Sore throat Bilateral pneumonia Ground-glass opacity Acute respiratory distress

observed in COVID-19 patients than that of SARS patients [12], [24]–[26].

E. DIAGNOSIS AND TREATMENT

The diagnosis of the virus is performed through a Reverse Transcription Polymerase Chain Reaction (RT-PCR) test. Another method that is used is the Computed Tomography (CT) scan which is considered to be a secondary method. The lungs of an infected patient are scanned and the resulted images of the CT scan should show the following irregularities (i) bilateral pulmonary parenchymal ground-glass, (ii) combined pulmonary opacities with spherical morphology, and (iii) a peripheral lung distribution [27]. In addition, the nucleic acid detection technologies include the real-time quantitative polymerase chain reaction (RT-qPCR) and high throughput sequencing. Meanwhile, the other auxiliary examinations include Point-of-care Testing (POCT) of IgM/IgG, enzyme-linked immunosorbent assay (ELISA), and blood culture [27]. The current treatment of Covid-19 is being carried out by using the following drugs and/or methods.

1) DRUGS

To treat COVID-19, some antiviral drugs have been practiced, e.g., 'ritonavir & lopinavir regimen' and 'remdesivir & chloroquine regimen' [28]. While the development of an antiviral drug specifically for the treatment of COVID-19 is still in progress, some potentially available compounds for further investigation are reported which can inhibit the viral activity. The antiviral compounds like nucleoside analogues block viral replication and β-D-N^4-hydroxycytidine (NHC) can also inhibit multiple viruses as per recent reports [29]. Some studies have shown that apart from nucleoside analogues, neuraminidase, DNA synthesis inhibitors, and Chinese traditional medicines as effective alternative drugs [30]. Antibiotics and forced mechanical ventilation support have also been helpful in COVID19 patients [22].

Remdesivir is a common antibacterial drug that is an adenosine analogue, which leads to premature termination of the virus by integrating into novel viral RNA chains. The efficiency and effectiveness of remdesivir in comparison to other drugs (lopinavir/ritonavir) has been verified by testing it on animals, it enhanced the lung tissue damage by dropping MERS-CoV titers of the infected animals [31]. Remdesivir has also shown promising clinical response in another study [32] where it has been used to treat SARS-CoV-2 and two clinical trials in China have warranted verifying its therapeutic efficacy. Furthermore, some pharmaceutically prepared inhibitors and peptides have shown the potential for antiviral activity against the virus [32]. Chloroquine, on the other hand, increases the endosomal PH which is required for the fusion of the virus and hence can block the virus. Its antiviral activity is also evident from its property of interfering with the glycosylation of cellular receptors of SARS-CoV [28]. It has also been suggested that remdesivir with a combination of chloroquine in administered amounts was effective in suppressing the effects of 2019-nCoV [28]. Chloroquine phosphate, in addition to chloroquine, has also shown good results and adequate preventive features against COVID-19 associated pneumonia in clinical trials [33].

2) PLASMA TRANSFUSION

Convalescent plasma has been in news since the outbreak for the treatment of SARS-CoV and some studies have suggested that if the treatment is administered early after observing infection's symptoms, it can effectively reduce the time for hospital stay along with the mortality rate [34]. However, another study revealed that there is no significant improvement of plasma transfusion on the survival of Ebola-infected patients [35]. According to a study on plasma transfusion [36], five people donated their convalescent plasma with written consent provided. All of the five donors had been diagnosed with the COVID-19 virus and at the time of donating their blood, they had fully recovered from COVID-19 and had no other life endangering diseases as well. Their ages lie between 18 and 60 years. 400 mL of plasma was obtained and was transfused to five recipient patients on the same day. After the plasma transfusion, body temperature normalized within 3 days in 4 of 5 patients. Viral loads also became negative within 12 days after the transfusion. Three patients stopped depending on the ventilators within 2 weeks. Out of the five patients, three were discharged from the hospital and two became stable on the 37th day after transfusion.

3) VACCINE

The formulation of a perfect vaccine for the novel Coronavirus started a few months after the outbreak. Some studies have suggested utilizing previous vaccines or strategies for the development of the vaccine against SARS-CoV [37]. While other studies propose some vaccines which are under development to be effective [38]. The development of neutralizing antibodies has previously been studied as a treatment for SARS-Cov [39], [40]. In addition, noteworthy results were reported when mice and hamsters were subjected to recombinant protein from the Urbani

(AY278741) strain of SARS-CoV. The animal testing results in other studies [41-46] have shown a substantial reduction in viral infection due to DNA fragmentation which has inactivated the whole virus or a strain of SARS-CoV (AY278741). Some other strains of SARS-CoV have also been reported to produce inactivated vaccines which result in the reduction of the virus in animal model testing, efficiently. These strains include Tor2 (AY274119) [37], [47], Utah (AY714217) [48], FRA (AY310120) [42], HKU-39849 (AY278491) [49], BJ01 (AY278488) [50], [51], NS1 (AY508724) [52], ZJ01 (AY297028) [52], GD01 (AY278489) [52] and GZ50 (AY304495) [50].

However, out of all underdeveloped vaccines in the fight against SARS-CoV-2, there are a few which went into the trial phase. US National Institute of Allergy and Infectious Diseases has been working on the phase 1 trial of the mRNA based vaccine, for the treatment of the novel coronavirus [51]. Stamina Therapeutics and Shanghai East Hospital of Tongji University have also been working on testing and availability of mRNA-based vaccines [53]. The Chinese Centre for Disease Control and Prevention (CDC) is also currently working on and trying to develop an inactivated virus vaccine [54], [55]. A Modified Vaccinia Ankara (MVA) vaccine developed by GeoVax-BravoVax, is ready for animal efficacy testing and human clinical trials [56]. While a recombinant 2019-nCoV S protein subunit-trimer based vaccine has been developing by Clover Biopharmaceuticals [57]. However, some of the vaccines produced by a few pharmaceutical companies and some research institutions have successfully completed the trail phase and have gone into mass production for public availability. Pfizer-BioNTech and Moderna vaccines have been authorized by the U.S Food and Drug Administration (FDA) [58]. However, the vaccine Oxford–AstraZeneca [59] and around 58 other vaccines are in the clinical trial and experimentation phase [38].

4) EQUIPMENT FOR TREATMENT

As per the standard operating procedures designed by NHS-UK for intubated patients of COVID-19, infusion pumps, dispensers, oxygen and blood pressure monitors, syringe pumps, and ventilators are some of the major equipment to be present in isolated wards for the treatment of these patients [60]. The patients that reach their critical state in illness are required to be shifted to ICU on mechanical ventilators. The chances of recovery on ventilators for the patients are usually very thin. For quick recovery or prevention, it is indispensable to have a very precise diagnostic mechanism to detect small irregularities of the patient's vitals. Furthermore, due to the continuously increasing number of patients worldwide, the need for low-cost, easily accessible medical equipment is imminent. This increased demand has brought about the need for more precise, portable, and less expensive manufacturing technology, e.g., MEMS and micromachining. MEMS and micromachining are used for the manufacturing of sensors/actuators used in various patient monitoring and diagnostics equipment. Various MEMS devices and sensors are currently being used in biomedical equipment and are being manufactured by various commercial organizations and research labs. But its manufacturing is still limited and the industry-academia collaborations are needed more than ever to accentuate the advancement in these sensors on a commercial level.

5) REVIEW METHODOLOGY/APPROACH

This article reviews various MEMS sensors which are being used or have been proposed in literature for the applications related to the equipment used for the treatment of COVID-19. Section I presents a brief history and introduction of COVID-19 including spread trends, diagnosis, treatment and equipment used for its treatment. Section II has been divided into subsections, where each subsection is dedicated to a single equipment. The MEMS sensors have been reviewed according to different applications involved in each equipment, e.g., airflow detection and air pressure detection in the ventilator, blood pressure measurement, and temperature detection in the patient monitoring system etc. The comparison has been done on the basis of operating principle/mechanism, performance parameters (sensitivity, operating range, SNR etc.), and the application of the reported sensors. The sensors to be reviewed have been chosen on the basis of application, relatedness and performance parameters. Furthermore, some commercial sensors have also been taken into account. The fabricated sensors with experimentally validated results have been prioritized on the simulation based proposed sensors. Section III presents a comprehensive discussion on the reviewed sensors with advantages and limitations of the sensors. The discussion section also highlights the commonly used operating principles, best available sensitivities, and most suited sensor for a specific application. A summary of the reviewed sensors has also been presented in this section. The discussion is followed by a clear and concise conclusion in section IV highlighting the importance of the study with conclusive remarks.

II. MEMS SENSORS IN THE EQUIPMENT USED FOR COVID-19

MEMS devices (sensors/actuators) are extensively used in the field of biomedical and health sciences, therefore mostly referred to as Bio-MEMS. Their smaller size (1μm$\sim$1mm), negligible weight, cost-effectiveness, prompt response, precise measurements, high efficiency, and easy system integration make them suitable for many healthcare applications in disease diagnosis, prevention, and treatment. This section reviews and reports the important MEMS sensors (both research-based and/or commercially available) which are currently being used or can be used in the equipment for treating Covid-19 patients.

A. MICROFLUIDICS/PCR TESTING

Microfluidics (MF) deals with the flow of fluids (microliter to attoliters) within submicron-sized channels. This field mainly aims to develop lab-on-chip devices. Miniaturization

of electronic IC and MEMS [61]–[63] coupled to fluidic systems gave birth to microfluidics: a new discipline based on the flow of fluids (fluid mechanics) and suspensions in small scale systems driven by external forces. Manipulating fluids at the micro-scale changes relative importance between forces. Some important characteristic changes involved in microscale manipulation of fluids are given in Table 2 [64].

TABLE 2. Comparison of flow in macrochannels and microchannels.

Phenomenon	Macrochannels	Microchannels
Gravity	Dominant (typical size >> capillary length: l_c	Negligible (channel size <<l_c)
Reynolds number	Laminar and turbulent flow (Re ≈ 2000)	Laminar flow (Re<1) in most cases, Stokes flow approximation
Surface roughness	Negligible	To be considered; roughness may be comparable to dimensions of the system
Diffusion	Negligible	Important and used for separation and missing
Surface tension	Negligible	Important and major contributing force
Viscous heating	Negligible	Major player due to high-velocity gradient
Electrohydrodynamic effects	Negligible	Important

Microfluidics also holds significance and its application in fields of nanomedicine (new medicines at nano particles scale containing the biologics like peptide, proteins etc., and other drug molecules), drug delivery, and most prominently in the field of diagnostics [65].

With the help of microfluidics, several types of nanoparticles, e.g., virus-like particles (VLPs), poly lactic-coglycolic acid (PLGA) nanoparticles, liposomal nanoparticles etc., can be created. These nanoparticles can encapsulate various drug molecules, e.g., peptides, siRNA, etc., which can be utilized for COVID-19 [66]. It has been reported in various research findings that the COVID-19 disease affects T-cells in the body. Microfluidics here can be helpful in formulating the biocompatible particles which can deliver siRNA to activate the T-cells.

Microfluidic devices are also being used in testing the novel coronavirus using Polymerase Chain Reaction (PCR). PCR is a method in which target DNA is copied multiple times for further identification and testing. The DNA is firstly collected from the sample under consideration, it may be a hair follicle, any material from a crime scene, or an ancient bone or tissue. Typically the process is performed on a machine knows as a PCR machine or thermocycler shown in Fig. 2. The solution to be processed contains the target DNA sample, enzyme DNA polymerase, primers, nucleotides, the pH optimizing buffer, and $MgCl_3$ [67]. It involves the repetition of a series of three basic steps. In the first step, the temperature is increased to about 90^{o}C. This increase in temperature breaks the hydrogen bonds present in the DNA sample due to which it disintegrates into two single strands from double strands. In the second step, the

FIGURE 2. PCR Machine or also known as Thermocycler [68].

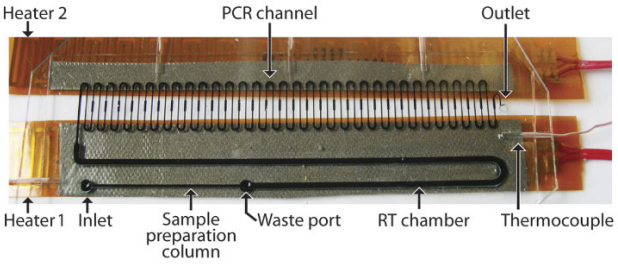

FIGURE 3. PCR testing microfluidic chip [71].

temperature of the solution is decreased to 55^{o}C – 60 ^{o}C, which causes the primers present in the solution to anneal to the individual DNA strands. Step three i8nvolves the increase in temperature to 72^{o}C to start the extension of DNA by using nucleotides and DNA polymerase. This three-step cycle is repeated many times to produce a large number of target DNA in the solution. After 30 cycles the DNA is multiplied to more than a billion copies of the original DNA. This whole process is done on a bulky thermocycler, usually costing several thousand dollars.

However, this whole process can be done on a microfluidic lab-on-chip with a very little price as compared to the conventional machine. The basic idea is to devise a method by which the three major steps of PCR are carried out on a single chip. For this purpose, some microfluidic devices were created with a miniaturized version of heating elements and fluidic pumps [69], [70]. These devices follow the general rules of standard PCR, i.e., the heating of solution for bond breakage, the culling down to react with primer, and the heating to replicate the DNA with nucleotides and DNA polymerase. A typical microfluidic PCR chip with the testing procedure is shown in Figs. 3 and 4 respectively.

In addition to the typical PCR tests, digital PCR is also being used in diagnostics of Covid-19. As reported, due to the high rate of false-positive and false-negative cases of PCR and reverse transcription PCR (RT-PCR), digital PCR

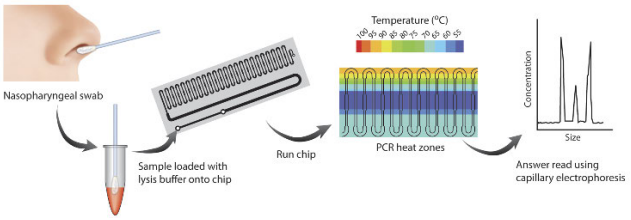

FIGURE 4. PCR testing procedure [71].

shows higher sensitivity and accuracy to detect the virus with fewer false negative and false positive results as compared to RT-PCR [72], [73]. This improved sensitivity and accuracy spotlight the utility of microfluidics in clinical diagnostic methods.

B. VENTILATOR

Ventilation, in medicine, is the process of providing artificial breathing support to a patient who can't breathe properly. The device used for the said purpose is called a ventilator. It moves breathable air into and out of the lungs by forced actions. The basic ventilation process of a typical ventilator with the position of sensors involved in the ventilation process is shown in Fig. 5. More than half of critically ill patients require mechanical ventilation [74].

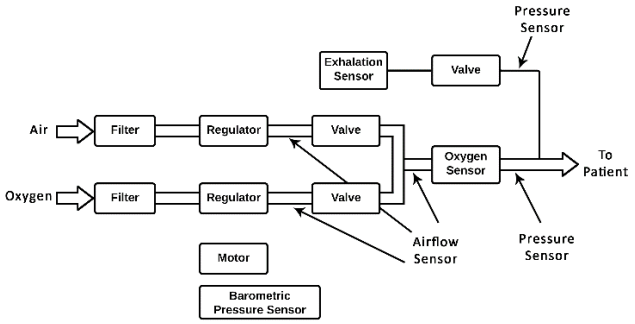

FIGURE 5. Basic ventilation process with the position of sensors and valves [75].

Ventilators are usually used in intensive-care units, life support systems in-home care, emergency medicine (as standalone units), and anesthesiology (as a component of an anesthesia machine) as well. Various types of ventilator systems have been under consideration during the COVID-19 pandemic. When the patients' condition becomes severe they experience acute respiratory distress syndrome which might lead to death. These patients require a ventilator to continue breathing because their lungs lose the capability to process oxygen and carbon dioxide partially/completely.

The important MEMS sensors used in currently used ventilators are the MEMS flow sensors and MEMS pressure sensors, whose placements in the ventilation systems are shown in Figs. 5 and 6 [76].

1) MEMS FLOW SENSORS

Flow sensors are typically used in monitoring flow rates of fluids and/or gas either towards the patient from the

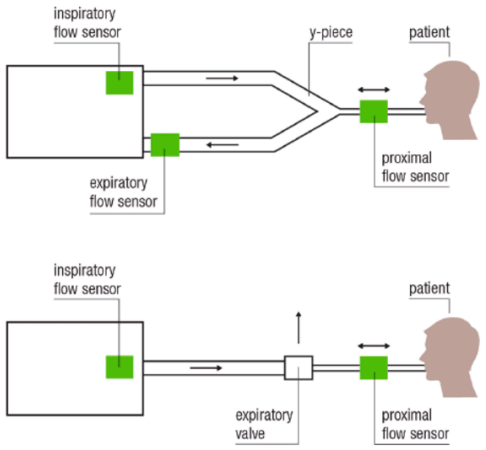

FIGURE 6. Placement of expiratory and proximal flow sensors [76].

outside environment or in reverse. MEMS flow sensors are small-sized low-cost devices capable of achieving high spatial and temporal resolution (from few micros to nanolitre per minute) with high sensitivity and accuracy in comparison to the traditional sensing devices [77], [78]. Researchers around the world have recently been more interested in the design and development of MEMS flow sensors due to their higher compatibility with semiconductor fabrication techniques and a higher packing density as an add-on [79]. These fundamental advantages make MEMS flow sensors desirable for applications involved in a ventilator. Apart from the ventilators, MEMS flow sensors also hold their importance in certain other important applications, e.g., the diagnostic devices, measurement of flow during biomedical surgery, in the fields of chemistry and therapeutics [80], liquid dispensing systems [81], [82], and also in gas monitoring systems [83], [84].

Flow sensing has always been challenging and crucial in a ventilator. Proximal and expiratory sensing in a ventilator requires a decent flow sensing technology. The proximal flow sensor serves a variety of applications including adult care and neonatal. Respiratory devices utilize proximal flow sensors to assist the noninvasive ventilation patients, intubated patients in hospitals, emergency rooms, and some cases of home care patients. These essential sensors require reliability and long term stability. Moreover, hygienic sterilization is another challenge due to the patient's continuous contact with air and the risk of pathogen infections. Sterilization of these sensors must be done carefully to avoid potential damage to the sensor during the sterilization process. Single-use sensors prove to be a better option because they don't need to be sterilized and can be replaced on each use, unlike conventional flow sensors that need to be sterilized with autoclaving or other methods. The MEMS-based single-use proximal flow sensors, shown in Fig. 7, is one such example of a fully calibrated reusable sensor. Unlike existing sensors, e.g., hot wire sensors etc., these new MEMS-based single-use proximal flow sensors don't require frequent calibration before or after being used and allow ventilator manufacturers

FIGURE 7. Single-use MEMS flow sensor [76].

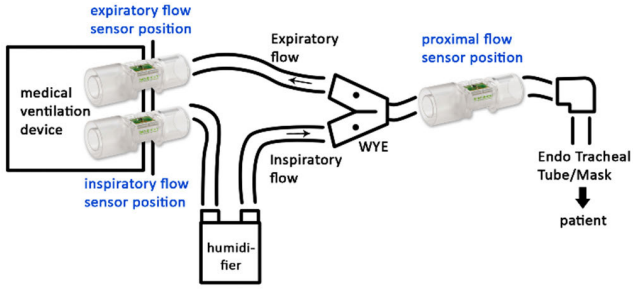

FIGURE 8. Position of single-use sensors in ventilators [87].

and their customers to spend less time on calibration [85]. The schematic construction of a ventilator with the position of these single-use sensors is shown in Fig. 8.

MEMS technology also improves repeatability and various other sensor characteristics, e.g., a commercially available solid-state MEMS airflow sensor reported in [86] removes the requirement of a surface cavity or a fragile membrane on the sensor die, making the sensor more robust and repeatable by using a piezoresistive sensor.

An important parameter involved in respiratory equipment is the flow rate measurement. MEMS-based flow sensors can be very precise in measuring nano newton flow rates. Flow sensors are broadly categorized as thermal and non-thermal sensors. Thermal sensors convert the heat transfer of the fluid flow into electrical signals, thus controlling the thermal behaviors of sensing components [88]. Whereas, the non-thermal sensors have different operating principles which include lift force, differential pressure, and deflection of cantilevers [89]–[92]. Important applications of thermal flow sensors in some cases include flow sensing and measurement of gas or liquid [93]–[104]. MEMS-based thermal flow sensors can measure liquid flow down to 0.05 l/min [105]. A comparison of non-thermal MEMS flow sensors is shown in Table 3 whereas, thermal flow sensors have been compared in Table 4.

Various micromachined flow sensors have been developed for applications such as inspired airflow, aspirated air flow and for certain other breathing characteristics. In this regard, for the measurement of breathing characteristics, an implantable catheter flow sensor has been developed [119]. The sensor has unique legs-like structures that help it in attaching to the walls of the air passage.

TABLE 3. MEMS non-thermal sensors for fluid flow detection.

Material	Fluid Type	Detection Range (m/s)	Sensitivity
Ti/Al resistor [106]	Air	0.01-0.03	NA
Polysilicon [107]	Air	0-6	7.4e-6 l/(m/s)
Al [108]	Air	0.7-21	0.65-4.49e-5 l/(m/s)
Cr/Pt [109]	Air	5-45	0.0284 ohm/(m/s)
Si (P type) Piezoresistor [110]	Air	20-40	0.204e-3 V/(m/s)

TABLE 4. MEMS thermal sensors for fluid flow detection.

Sensing element materials	Fluid Type	Detection Range (m/s)	Sensitivity
P-Doped Polysilicon Thermopile [111]	Air	0-50	3.04e-2 V/(m/s)
Pt Resistors [104]	Air	0-4e-3	1.44e-2 V/(m/s)
Ti/Au/Ti Heater [112]	Air	0.005-0.1	116.38 V/(m/s)W
Ni Resistors [113]	Air	0-30	2.93e-2 V/(m/s)
Cr/Pt Resistor [114]	Air	0.016-0.167	9.4e-3 V/(m/s)
Poly-Si Micro Heater [115]	Air	0-11	230 V/(m/sW
Ti/Ni Resistor [116]	Gas, N2	3-237	1.35e-3 V/(m/s)
Pt Sensing Element [117]	Gas	0-0.01	2.137 V/(m/s)
W/Ti/Pt Sensing Element [96]	DI water	1.33e-02	2.14e-6 V/(m/s)
Luminescent Sensor Layer [118]	liquids	4.5e-4 -0.457	216.5 K/(m/s)

The presented sensor uses hot-wire anemometry sensing mechanism for flow sensing. The sensor is tested by implanting it inside the bronchus of a rat and a rabbit. The measured breathing characteristics and waveforms are coincident with the mechanisms of breathing. The sensor has a response time of 0.23s and has been tested for breathing frequency range of 0.63 Hz to 1.9 Hz. Fig. 9 shows fabricated sensor film, the shape of the attachable legs, and the implantable catheter sensor attached inside the air passage with the help of the designed legs.

During the ventilation process or specifically during the volume-controlled ventilation, an airflow with positive pressure is used in inflow and outflow directions. This positive pressure results in an unrestrained stress on the lung tissues and this stress usually ends in causing a ventilator related lung injury (VALI). Hence, to avoid such injuries caused by the positive pressure airflow of the ventilator, a sensor is required to measure the pressure in the lungs. To address this issue, a respiratory monitoring system is developed by Yoshida *et al.* [120] to evaluate elasticity of the lungs due to the positive pressure airflow. A MEMS tube-type thermal flow sensor has been fabricated and used with other commercially available Si-MEMS pressure sensors. The developed system has been placed between a rat's lung and the ventilator to evaluate the elasticity of the rat's lungs. The flow

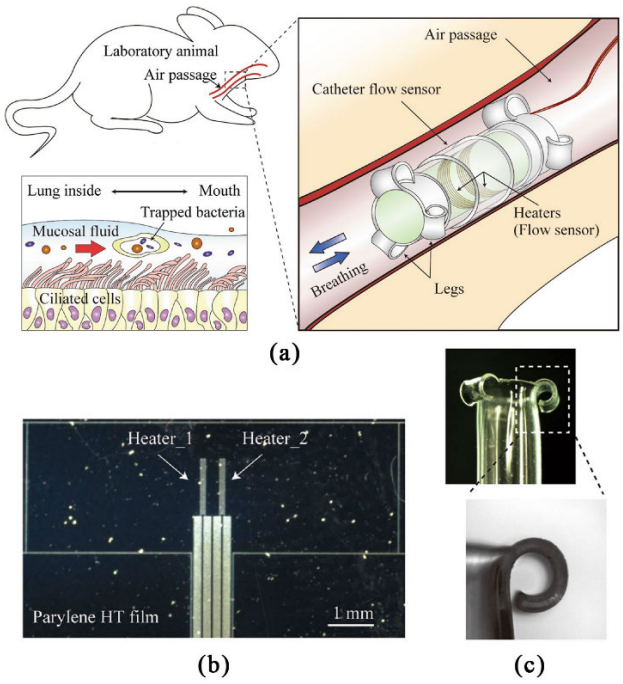

FIGURE 9. (a) The catheter flow sensor implanted into air passage of test animal, (b) Optical Image of the fabricated sensor film, (c) Shape of the attachable sensor leg [109].

volume vs. pressure waveforms are obtained which correspond to the lung elasticity of the rat. The developed respiratory system proved to be a viable solution to avoid ventilation related injuries.

An ultra-low airflow velocity flow sensor is designed, developed and tested in [121] which is capable of real-time detection of airflow velocity of just a few millimeter per second. Microscopic hair like structures have been fabricated from polymer. Polymer gives them the properties like being flexible and conductive, due to which they can promptly respond to air flowing over them. The experiments show the sensing ultra-low velocity sensing capability of 0.66 to 0.97 m/s.

A MEMS thermal gas flow sensor is designed and fabricated in [122] which has an additional capability of self-test function. The sensor's design consists of a heater in the centre with thermopiles surrounding the heater. The sensor has been tested by measuring flow characteristics of nitrogen gas and boasts a high sensitivity of 123 mV/(m/s)$^{-1}$ with a response time of just 250ms.

A MEMS liquid crystal polymer (LCP) flow sensor is presented in [123]. This sensor is used to sense critical flows related to intravenous (IV) infusions. The sensor has a liquid crystal polymer membrane which is circular in shape having 2 mm diameter and 25μm thickness. The membrane has hair like structures at its center which help in flow rate measurement. This LCP membrane makes this sensor highly sensitive for measuring flow velocities as low as 2 mL/hr.

Speaking of flow sensors which are cost-effective and are made with the easily available and fully developed fabrication process, the sensors having silicon-based diaphragm membranes mechanism are widely used in biomedical instruments and are adequately sensitive [124]. Other than silicon, polymeric diaphragms have also been drawing attention recently because they tend to be biocompatible, flexible, less expensive with other important mechanical properties [125].

To develop highly sensitive and accurate flow sensors, researchers have also been exploring the nature to develop biomimetic flow sensors by understanding and applying the sensing and basic design principles of the biological flow sensors that exist in nature [126]. For example, recently a fish inspired MEMS flow sensor has been presented having a biomimetic cupula [127]. The developed sensor is used for the steady-state and oscillatory flows. Experimental results depict the accurate measurement of the steady state flows and the use of the cupula structure enhances the sensor output for the oscillatory flows. This sensor validates the role of biomimetic structures in improving the sensitivity and performance of the MEMS sensors.

2) MEMS PRESSURE SENSORS

The MEMS pressure sensors hold huge importance in respiratory monitoring and are used in the ventilators to monitor a patient's breathing [128]. Pressure sensors are critical components in ventilators and provide necessary breathing assistance to patients battling COVID-19. During the process of inflating a patient's lungs properly, the pressure needs to be carefully monitored and normally it is kept relatively low (typically 10 cm H_20). Since the ventilators are only employed for critically ill patients in serious life-threatening situations, accuracy and high performance are desired. Therefore the ventilator manufacturers are advised to use the most precise pressure sensors while developing the ventilators [75].

MEMS-based pressure sensors contribute to the advancement and improvement of conventional ventilators to avoid various injuries involved during the ventilation process. Mechanical ventilation escalates the time needed for recuperation and can cause ventilator-associated lung injury (VALI) and ventilator-induced lung injury (VILI) due to overdistention of lungs. To reduce potential lung injury, asynchrony between the patient's efforts, and the ventilator should be reduced. MEMS-based piezoresistive sensors prove to be quite helpful in this scenario. These sensors are used to measure pressures in Endo Tracheal Tube for the identification of breathing efforts initiated by the patient. The response is fed back to the ventilator so that the ventilator can regulate its ventilation modes and tidal volumes according to the provided response [74]. Furthermore, due to the small sizes of the aforementioned MEMS-based sensor, the injury-prone situations are much reduced.

In addition to the airflow and pressure, another important parameter in ventilators is the measurement of oxygen flow. The disruption in the provision of oxygen happens when the patient's condition deteriorates over time. To stabilize the patient's condition, usually, a High-Flow Nasal

Oxygen (HFNO) is given using High Flow Nasal Cannula (HFNC) [129]. If the oxygen is not supplied to the patient in time, the organs start to work abnormally towards complete dysfunction. A feasibility study of a pediatric ventilator system was performed by Rajavelu *et al*. [79] with the usage of differential pressure as an operating principle for the measurement of oxygen flow. In the system, two micro pressure sensors were integrated with a meso channel. This arrangement resulted in the achievement of 90% better deflection and sensitivities of the sensor, 135% better stress generation, and managed to get 40% perforated area even if the diaphragm has been thicker validating the choice of thicker diaphragms over very thin non-perforated diaphragms for better performance. The study also validates the integrated meso channel/micro sensors design. Such advances in the development of MEMS pressure sensors have helped in the improvement of medical equipment for required applications.

From the research sector, the MEMS-based pressure sensors have made their way to the biomedical industry by producing comparable results. Kaisti *et al*. [130] suggested using an array of MEMS-based pressure sensors for health monitoring. This sensor array is shown in Fig. 10 is used to measure heart rate and radial artery pulse. The sensor elements are configured as an array and can be used in wearable devices. The used sensor has a measuring range of 30-120 kPa and is also suitable for other biomedical applications. It has a capacitive sensing mechanism in which a silicon wafer is used as a diaphragm that bends due to external pressure.

FIGURE 10. MEMS pressure sensor array for health monitoring [130].

A cardiological implantable device is also reported in [131] with the combination of CMOS circuitry and monolithically fabricated MEMS pressure sensor. The reported sensor is a capacitive MEMS pressure sensor that works by measuring the deflection of the flexible top plate. The sensors have been characterized using Atomic Force Microscopy (AFM) in contact mode. The cross-sectional view of the MEMS pressure sensor showing the deflection of the top plate is given in Fig. 11, whereas the SEM image of the fabricated sensor is given in Fig. 12. Another high sensitive CMOS MEMS rectangular capacitive pressure sensor is reported in [132]. This sensor is fabricated using the SiGeMEMS process (Silicon-Germanium MEMS process). Polycrystalline Silicon Germanium (Poly-SiGe) is used as the sensor diaphragm. The diaphragm has a wide dynamic range, i.e., 2hPa to 500 hPa. This wide range helped in an increased low-pressure capability for the pulmonary wedge pressure measurement.

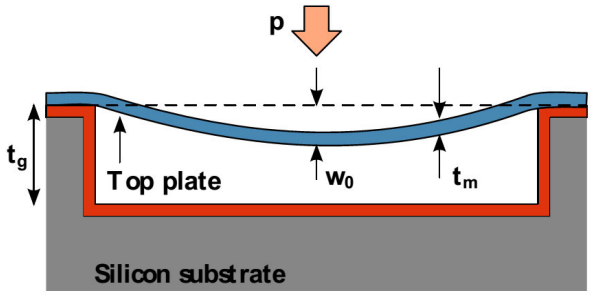

FIGURE 11. The cross-sectional view of a MEMS capacitive pressure sensor [131].

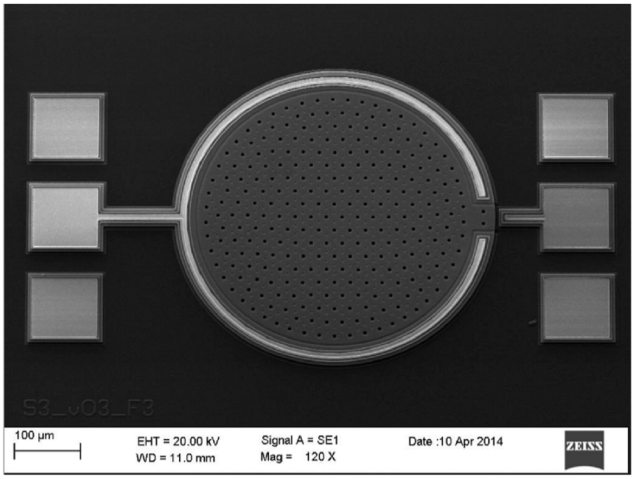

FIGURE 12. SEM of the fabricated sensor [131].

For a full scale range of applied pressure, the sensor exhibits a minimum non-linearity of less than 1% with an adequately high sensitivity of 8.72 mV/V/hPa.

The reported design improvements and rapid commercialization has resulted in the improvement of the medical equipment available today. As mentioned in this section, MEMS pressure sensors have almost revolutionized the available equipment in terms of portability, miniaturization, and small scale measurement.

C. PULSE OXIMETER

As discussed earlier, COVID-19 patients experience a lack of oxygen in their lungs, which disturbs the oxygen supply to the whole body and other organs as well. This low oxygen level in the bloodstream or tissues is termed as Hypoxemia [133]. One of the distinctive features of Covid-19 pneumonia is severe hypoxemia [134]. In the case of COVID-19 patients, continuous measurement of oxygen levels is essential. Pulse oximetry provides an accurate and non-invasive diagnosis of hypoxemia conditions [135]. Diagnosis solely based on clinical symptoms usually lacks accuracy in predicting hypoxemia, whereas pulse oximetry results in 20-30% more correctly diagnosed hypoxemic cases [136]–[138]. Additionally, identification of hypoxemia based on clinical symptoms of severe pneumonia, often by nonphysician clinicians or community health workers,

remains inconsistent and unreliable [139]–[142]. Therefore, a pulse oximeter serves a useful function in the treatment of Covid-19 patients, not only for measuring oxygen saturation but for respiration rate and pulse wave as well.

Various implantable MEMS-based oxygen sensors have been proposed and developed in the literature for oxygen measuring at a fixed position [143]. A study by Bingger *et al.* [144] has reported the design and operation of an implantable MEMS-based optical sensor manufactured by utilizing micromachining techniques. The designed sensor is capable of continuous long-term monitoring of arterial blood oxygen saturation pulse and respiratory frequencies. The sensors have two elastic silicon strips to be wrapped around the blood vessels as shown in Fig. 13. The arterial blood vessels are enfolded by these elastic strips in such a way that they don't constrict the vessel or disturb the blood flow, even at large dilatations of 10%. The sensor was placed around the carotid artery of a domestic pig for *in vivo* measurements. The results show excellent data of real-time measurement during the testing. The experimental results validate the possibility of monitoring the pulse, along with pulse shape & respiratory frequencies, and also the blood oxygen saturation. The prototype of the oximeter is shown in Fig. 13 and the cross-sectional design is given in Fig. 14.

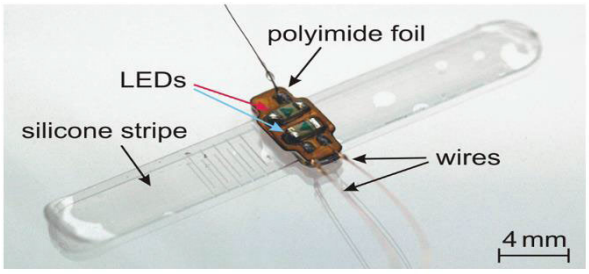

FIGURE 13. The prototype of the Implantable MEMS optical sensor pulse oximeter [144].

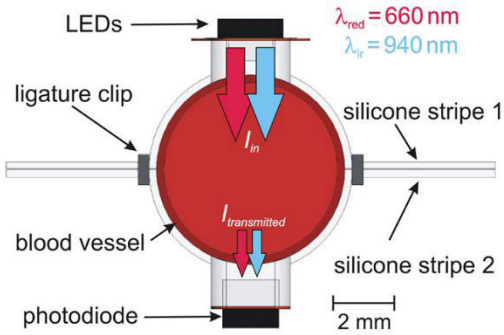

FIGURE 14. The cross-sectional view of the sensor [144].

A MEMS-based implantable oxygen sensing system is reported in [145]. A biocompatible and biodegradable oxygen sensor is developed and the system is optimized specially for the long-term monitoring of oxygen. For testing purposes, in vivo oxygen levels in mouse gluteus muscle and zebrafish trunk muscle have been successfully measured and investigated. For the fabrication of the oxygen sensor, PDMS (Polydimethylsiloxane) is used as the oxygen-permeable membrane. The fabricated sensor is shown in Fig. 15. Such sensors are extremely useful in situations like COVID-19 where continuous/long-term measurement of oxygen levels is indispensable.

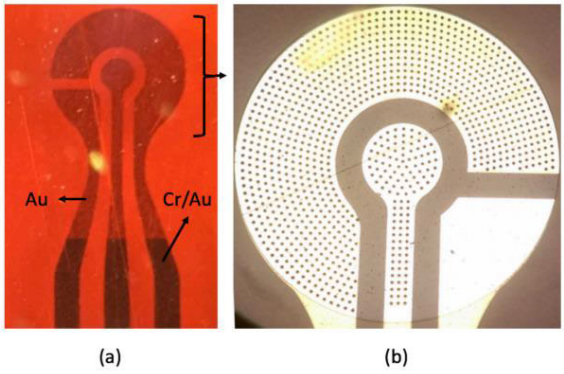

FIGURE 15. (a) Optical image of sensor electrodes (b) Top view of MEMS biocompatible oxygen sensor [145].

A respiratory monitoring and training system based on MEMS magnetic sensor design is presented by Oh *et al.* [146]. The components of the presented system comprise a sensor, a magnet, and a breathing pattern output device. The parameters for performance analysis of the system include the amplitudes of respiration cycles, magnet's position angles, and error. The results have shown that the designed system utilizes the advantage of an additional magnet while comparing it to conventional sensing methods and have been accurate in its breathing signal graph with the least measurement error and higher spatial resolution.

For blood pressure measurement and waveform sensing in pulse oximeters, a typical method is the use of infrared photoplethysmogram (PPG). The recently opted alternative of PPG is the pressure sensing method. Various pressure sensing elements have been developed for the said purpose even for long term blood pressure monitoring. A pressure sensor array attached to a wristband has been developed in [130] for radial artery pulse measurement and heart rate detection. The sensor used in the device is Murata's capacitive pressure sensor (SCB10H). It has two silicon wafers and one glass wafer. One of the silicon wafers is used as a diaphragm that bends on external pressure and capacitance is measured. The sensor has a measuring range of 30-120kPa with a sensitivity of 55fF/kPa. The device is tested on 13 healthy subjects and from each subject, the average arterial waveform is obtained successfully. The obtained waveform also displays the diastolic and systolic peaks.

Another study has been carried out for designing a pulse wave measurement method using a MEMS cantilever based sensor [147]. The design has a thin piezoresistive cantilever of a thickness of 300-nm as a membrane inside the air chamber of sensors. The pulse wave tends to deform whenever there

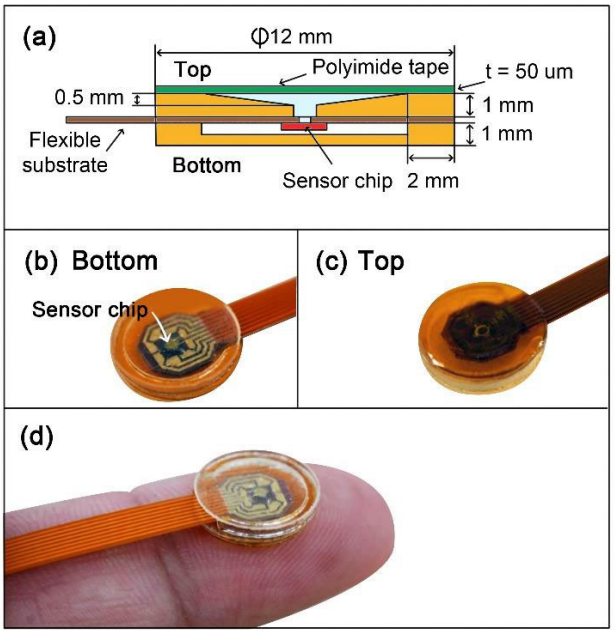

FIGURE 16. (a) Device layout with sensor chip, (b) bottom view of the fabricated sensor, (c) top view of the fabricated sensor and (d) scale of the sensor as compared to an index finger [147].

is a contact between a subject's skin above a vessel and the membrane, triggering a change in the chamber pressure. This pressure change can make the cantilever bend, hence changing its resistance. The resistance of the cantilever has been used to monitor and measure the pulse wave of the subject. The presented device with its cross-sectional view is shown in Fig. 16. The designed sensor is also fabricated and validated by measurement of the pulse wave velocity (PWV). The investigation results have shown a pretty good possibility of continuous blood pressure measurement using the designed and fabricated sensor.

Another pulse wave measurement design approach is proposed by Nguyen and Ichiki [148]. The designed sensor can measure the respiratory rate as well as the measurement of blood pulse wave rate using the same sensor. In the proposed device, a piezoresistive cantilever is placed inside a thin silicone tube for the measurement of the inner pressure as shown in Fig. 17. It is particularly attached to the nose pad of an eyeglasses pair. The sensor utilizes a differential pressure mechanism. The response of the sensor with the depiction of the differential pressure mechanism is shown in Fig. 18.

D. SYRINGE/INFUSION PUMP

A syringe/infusion pump is an intravenous fluid controlling device that is used for injecting drugs in a predetermined and consistent manner. These pumps are regularly used in delivering insulin, antibiotics, chemotherapy drugs, nutrients and pain relief drugs, etc. Most of the hospitalized patients in intensive care units receive IV therapy through syringe and infusion pumps. A typical syringe pump with labeled components is shown in Fig. 19. For larger volumes of drug

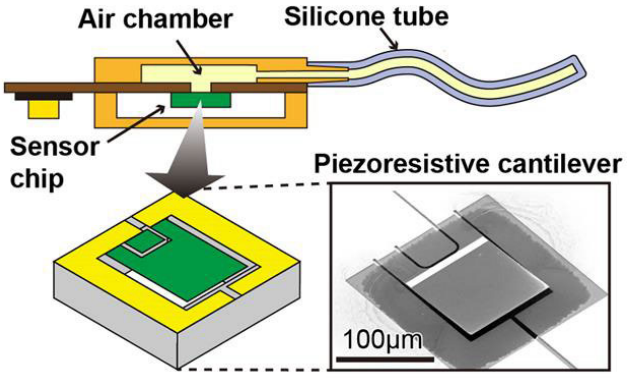

FIGURE 17. Layout of the pressure sensor for pulse wave and respiration measurement using a single silicone tube shaped sensor which is attached to an air chamber [148].

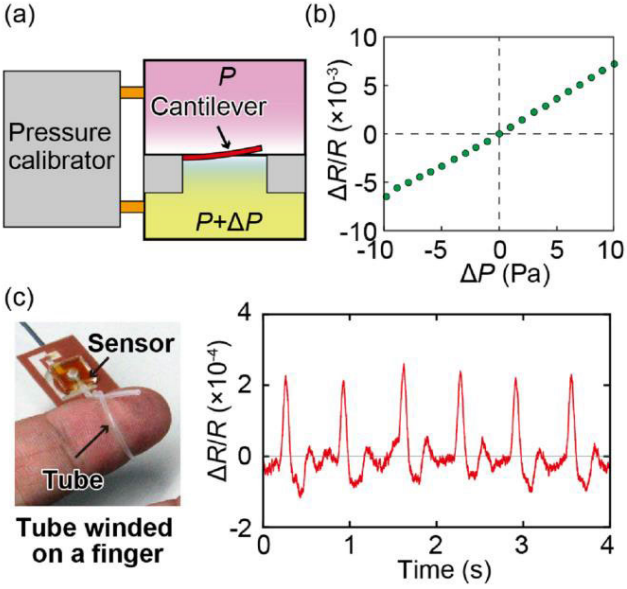

FIGURE 18. (a-b) Differential pressure being applied to the top and bottom of the cantilever for calibration (c) Response of the sensor when the tube is wrapped around the finger [148].

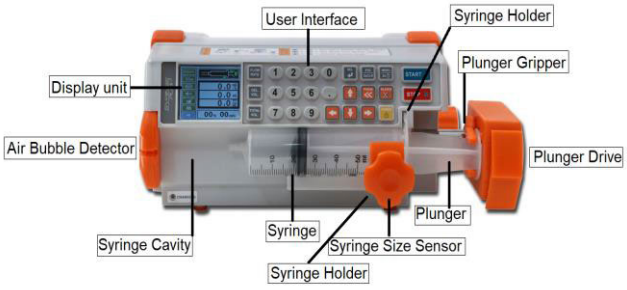

FIGURE 19. Syringe pumps for IV infusion [149].

infusion, volumetric infusion pumps are used. For accurate administration of intravascular drugs, fluids, whole blood, or blood products, infusion pumps can be utilized with much accuracy as they can regulate fluid up to 2000 ml, having flow rate range of 0.1–2000 ml/h.

To receive the best intensive care in ICUs, the sensors in these pumps play a vital role. The amount and rate of the drug being delivered are solely dependent on the performance of the sensors inside. A minor increase/decrease in the amount of flow rate of the critical drugs being delivered may cause causalities. Therefore, precise readings from the sensors must be fetched. Due to an error in these sensor readings, the patient's vitals can abnormally change [150]. The important MEMS sensors used in the syringe or infusion pumps are force sensors, pressure sensors, and position sensors. A typical setting of an infusion pump with the position of all three sensors, i.e., the force sensor, the board mounted pressure sensor and the position sensor is given in Fig. 20. The design and the type of each of these sensors vary depending on the type of syringe or infusion pump. This section reports some commercially available and research-based force and pressure sensors.

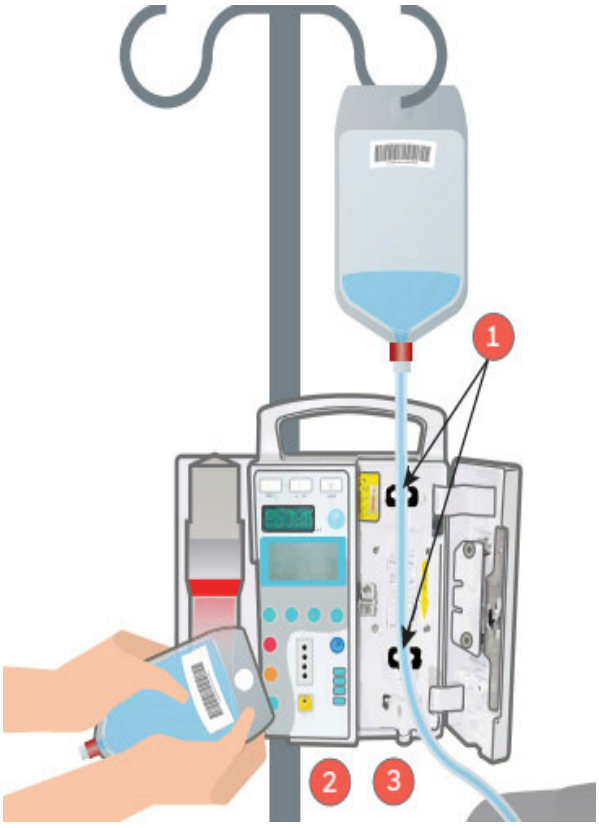

FIGURE 20. A typical Infusion Pump showing position of sensors being used (1) Force sensor, (2) Board mounted pressure sensor, and (3) Magnetic position sensor [151].

The commonly used and commercially available MEMS force sensors which are used in infusion pumps come from Honeywell. The force sensors from Honeywell are available in MicroForce FMA Series, FSA Series, FSG Series, FSS Series, FSS-SMT Series, TBF Series, and 1865 Series, etc. [151]. Honeywell sensors use micromachined silicon sensing elements. These sensing elements are piezoresistive, i.e., their resistance varies when the resistors flex under an applied force. The applied force is concentrated on the silicon sensing element by using a stainless steel ball. The resistance of the sensing elements actually increases proportionally to the amount of the applied force. This increase in the 'sensing element resistance' results in the change in the 'circuit resistance', which in turn changes the output voltage levels. A sophisticated Wheatstone bridge circuit design is used to provide stable voltage levels at the output for a given force range. The dimensional layout of a Honeywell force sensor FSS series is given in Fig. 21.

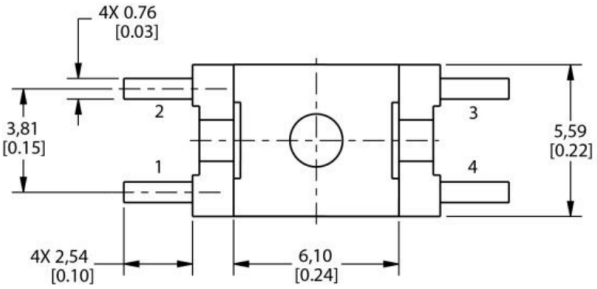

FIGURE 21. Honeywell force sensor FSS series layout with dimensions [151].

Some MEMS force sensors based on amorphous carbon (a-C) films with controlled piezoresistive behavior are presented in [152]. The sensors have been fabricated using DC magnetron sputtering technique. The sensitivity of these reported force sensors is 80.7 μV/V/N in the force range of 0 to 1.16 N, with a full scale nonlinearity of $\sim$1.3%. These force sensors display good repeatability of 5000 cycles.

A MEMS force sensor based on PDMS (Polydimethylsiloxane) microcantilever is designed and analyzed in [153]. The design focuses on sensing low magnitude forces (in μN range). For the enhancement of sensitivity, various combinations of stress concentrated regions (SCR) have been incorporated on the microcantilever. A sensitivity of 1.62 mV/μN in the range of a 0-100μN force is reported.

Apart from the force sensors, the commercially available pressure sensors used in syringe or infusion pumps belong to TruStability RSC Series, HSC Series, or SSC Series [151]. The TruStability pressure sensors have piezoresistive silicon sensing elements. These sensors have quite high sensitivity and have the capability to sense very minute pressure changes. Moreover, these sensors provide very stable digital output values.

Major system blocks of the sensor include; 1) a piezoresistive sensing element to sense the pressure and generate a signal, 2) an analog to digital converter (ADC) with an integrated amplifier that measures the generated signal, 3) an onboard EEPROM Memory that saves the coefficients for compensating equations, these equations help in correcting the originally generated signal to provide a pressure calibrated and temperature compensated value. The block diagram of a TruStability RSC series pressure sensor is given in Fig. 22. These sensors have a pressure range of $\pm$160Pa

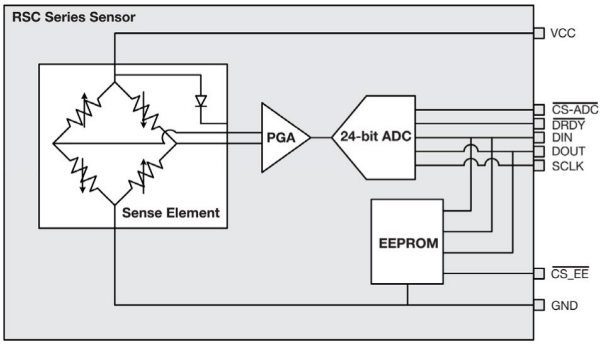

FIGURE 22. Block Diagram of a TruStability RSC series pressure sensor [151].

to ±1 MPa and are extensively used in airflow monitors and anesthesia machines.

A CNT (carbon nanotube) based scalable and integratable piezoresistive pressure sensor is reported in [154]. It has a CNT conductive network and a photoresist insulation layer. The reported pressure sensor offers a sensitivity of 95.5 kPa^{-1}, a low sensing threshold of 16Pa, a fast response speed of less than 16ms. Moreover, this sensor consumes no power when the loading pressure is not being applied. The operating mechanism of the reported sensor is shown in Fig. 23. When the sensor is pressed, the two layers of carbon nanotubes are deformed and these layers sink into the holes of the photoresist layer. When the applied pressure increases and passes the sensing threshold, the two electrodes come into contact with each other and the current starts flowing between them. As the pressure increases further, the contact area of the two layers is also increased and the value of current also increases. By varying the thickness of the insulation layer and the diameter of the holes, the parameters like dynamic range, sensitivity and the sensing threshold can be tuned. The fabricated pressure sensor is highly sensitive and has been reported to be suitable for applications like artificial skins and wearables. The improved sensitivity and low sensing threshold make it suitable for various biomedical equipment including syringe/infusion pumps to measure low pressures.

A graphene piezoresistive MEMS pressure sensor is presented in [155]. The presented sensor has been analyzed for different values of temperature. The sensitivity of the presented sensor is 3.98 mV/psi on room temperature and doesn't vary significantly on increasing the temperature. The graphene pressure sensor has been compared with polysilicon pressure sensors and it is validated that the sensitivity of the polysilicon sensors deteriorates significantly on the increase in temperature whereas, the graphene sensor shows a minute sensitivity variation of 0.02 mV/psi. This shows that graphene pressure sensors can be used at high temperatures.

E. PATIENT MONITOR

A patient monitor is usually used to draw cardiograms, to measure and display blood pressure (invasive or non-invasive type), respiration rate, temperature reading, oxygen saturation rate (SpO2), and pulse/heart rate. It is also used to monitor the patients on patient transport vehicles, and the measured information of the patient's condition is stored for further use at the hospital.

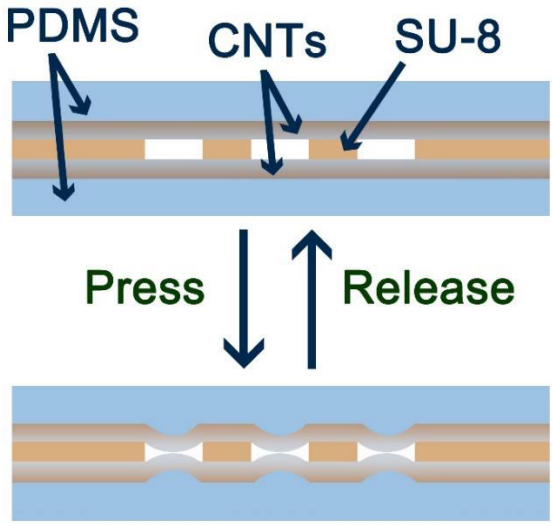

FIGURE 23. Schematic of the pressure sensing mechanism [154].

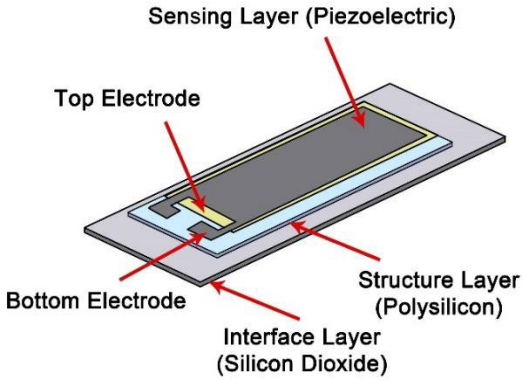

FIGURE 24. MEMS piezoelectric blood pressure sensor [156].

MEMS-based blood pressure measurement sensors are being used in various portable medical equipment. Two such sensors are shown in Fig. 10, previously in the pressure sensors section [130] and in Fig. 23. The piezoelectric cantilever based blood pressure sensor shown in Fig. 24. is reported in [156]. It proves to be a viable replacement for conventional bulky blood pressure measuring systems. The presented blood pressure sensor has three layers, i.e., an interface layer, a structural layer, and a sensing layer. The interface layer is made of silicon dioxide for isolation purposes, the structural layer is made of polysilicon for good contact of electrodes and the sensing layer is made of piezoelectric materials for sensing the blood pressure. The sensor has been analyzed for three piezoelectric materials, i.e., Barium Sodium Niobate, Bismuth Germanate, and Lead Zirconium Titanate (PZT).

The best performance is obtained by using Lead Zirconium Titanate exhibiting 4.95μm deflection of the cantilever and 2.52 V generated at the output at normal human body blood pressure (80 mmHg). The sensor shows high sensitivity and is suitable for non-invasive measurement of blood pressure.

A MEMS-based clamped capacitive pressure sensor for blood pressure measurement is designed by Rao *et al.* [157]. The operating range of the presented pressure sensor is 0-0.16 MPa. A diaphragm deflection mechanism has been utilized which in turn changes the capacitance between the diaphragm and the bottom electrode. The diaphragm and the bottom electrode, are made of Aluminum. A maximum deflection of 0.4μm is observed at 0.16 MPa. At the maximum deflection of the diaphragm, a capacitance of 59.644 fF is recorded. The designed sensor has a sensitivity of 7.97 fF/bar. This sensor is suitable for continuous/long-term measurement of blood pressure.

A novel piezoresistive MEMS pressure sensor based on temporary bonding technology is reported in [158]. The sensing membrane is fabricated on the device layer of an SOI (Silicon-On-Insulator) wafer. This wafer is further bonded to a borosilicate glass (BF33) wafer for the support. The size of the sensing membrane is 100μm$\times$100μm$\times$2μm. the operating range is 0-180 kPa with a sensitivity of 36μV/(V.kPa). The pressure sensor displays good linearity of 0.141% in the range of human body temperature. The fabricated sensor can be mounted in a medical catheter for blood pressure measurement. The design and SEM image of the fabricated sensor is shown in Fig. 25.

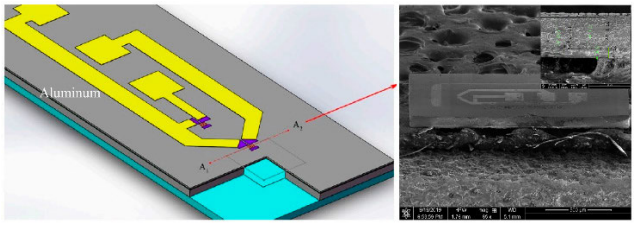

FIGURE 25. Design and SEM image of Piezoresistive MEMS pressure sensor [158].

In addition to blood pressure measurement, continuous body temperature sensing is critically important, especially in COVID-19 patients.

A MEMS resonator-based thermometer system on chip (SoC) is presented in [159]. The resonator sensor is fabricated using the UMC 0.18μm 1-poly-6-metal CMOS-MEMS process and is monolithically integrated with the readout circuitry. The mechanical resonator has two comb finger structures for driving and sensing, as shown in Fig. 26. In addition to these comb fingers, it has a moveable shutter structure to form mechanical resonance. For the readout circuitry, a high gain low power trans-impedance amplifier (TIA) and phase-locked loop (PLL) have been designed. The designed thermometer has an operating range of -40 to 120 °C with a sensitivity of -5.7 Hz/ °C or 0.224 mV/OC. the power consumption of the readout circuitry is only 190.4μW.

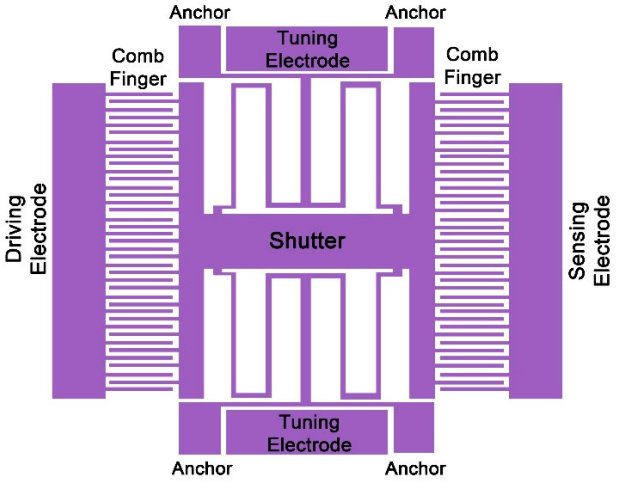

FIGURE 26. The top-view of monolithic resonator-based MEMS thermometer [159].

The aforementioned resonator-based MEMS thermometer is integrated with a real-time clock (RTC) in [160] for temperature compensation in addition to measuring temperature. A counter is used to count the resonator frequency and the value of temperature is converted into digital data without any need for additional analog to digital converter (ADC). The two main purposes of this modified thermometer are 1) to convert the analog temperature input into digital output without using the PLL and ADC circuit, 2) to develop a temperature compensated RTC for stable temperature response. The modified thermometer has a temperature range of 0-100 °C.

For temperature measurement, a low-cost flexible skin with multi-arrayed MEMS sensors has been developed by Xiao *et al.* [161] on a polyimide substrate. A liquid polyimide is used to make a flexible film on a silicon wafer. For temperature sensing, the arrayed micro temperature sensors are made from 0.12μm sputtered platinum thin film. An array of 8$\times$8 platinum thin films are micromachined on the polyimide and the silicon wafer is removed at the end of fabrication. The fabricated flexible temperature sensing skin is shown in Fig. 27, it can be attached to any flat, curved, rigid, or soft surface.

The rest of the sensors, respiration rate, and oxygen saturation measurement being used in the patient monitoring system have been discussed in previous sections.

F. ECG

An Electrocardiograph machine (ECG machine) is an electronic device used for monitoring the electrical activity of the heart. It provides essential diagnostic information about the heart's health. In a standard commercially available ECG machine, bioelectric signals are recorded using the bio-potential electrodes made of Ag/AgCl. A conductive interface is created between the electrode and human skin with the help of an electrolytic gel, referred to as the ''wet electrode''. Some limitations are also observed during the

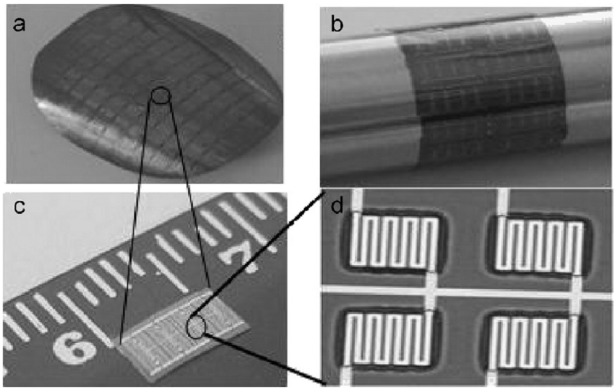

FIGURE 27. Micrographs of the sensor skin: (a) the flexible temperature sensing skin with multi-arrayed sensors, b) the flexible sensor skin wrapped around a stainless steel cylinder, (c) size depiction of the sensor array, and (d) four sensor arrays zoomed in [159].

process: 1) skin is sensitive and the process can cause skin abrasion therefore skin preparation is required. 2) Applying gel repeatedly can be a time-consuming task along with being inconvenient and uncomfortable for a person in some cases [162].

To avoid such inconvenience, MEMS-based electrodes prove to be a decent choice, which can be operated without using an electrolytic gel, and are therefore referred to as ''dry electrodes''. Instead of creating an electrochemical electrode-electrolyte interface, these electrodes utilize the capacitive detection principle. Another method of avoiding skin preparation is reducing the impedance between electrode and skin. For this purpose, a novel micromachined electrode based on hollow microneedles is developed by Yu *et al.* [162]. The electrode has been designed especially for the measurement of ECG signals. The schematic of this bio-potential electrode with hollow micro-needles is shown in Fig. 28. It consists of two layers, i.e., one layer consists of a silicon die having a hollow microneedle array and the other layer is a polymer die comprising the platinum (Pt) electrodes.

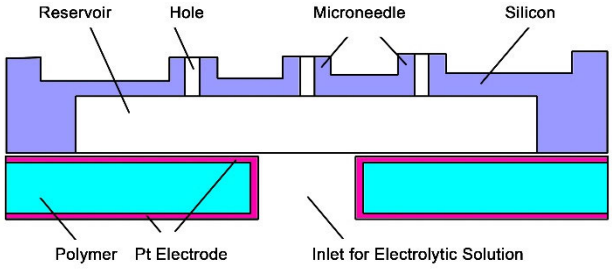

FIGURE 28. The schematic of the bio-potential electrode with hollow microneedles [162].

As the micro-needle array has been fabricated using silicon, it reduces the electrode-skin-electrode-impedance (ESEI) while piercing through the outer skin surface (consisting of dead cells). Another important feature of this device is that instead of electrolytic gel, the hollows of electrodes

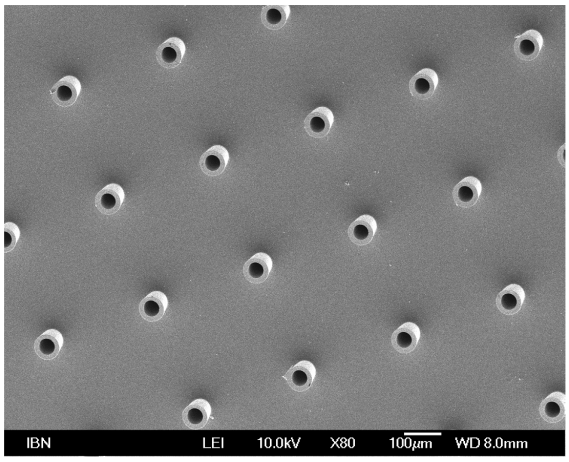

FIGURE 29. SEM picture of fabricated hollow microneedles [162].

have been filled by a salt solution in the reservoirs etched on the back of the silicon die. The presented device is potentially more comfortable, cost-effective, and convenient for ECG measurement and imposes no side effects on the human body. The fabricated microneedles have a diameter and depth of 100μm each. The SEM image of the fabricated microneedles is shown in Fig. 29.

The results of the microneedles based electrodes agreed well with the signals generated by the commercial wet electrodes. Fig. 30 shows the ECG signal extracted by using the microneedles based electrode. The fabricated electrodes can be integrated with a wireless communication device to construct a portable ECG recording system. The microfabricated bioelectrodes make this system capable of continuous, long-term, and repetitive ECG measurements.

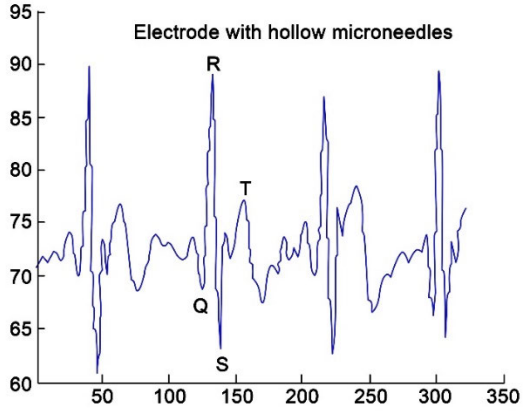

FIGURE 30. ECG signal measurement from the biopotential electrode with hollow microneedles [162].

Another important contribution to ECG measurement methods is the development of flexible ECG sensors. In this regard, MEMS ECG sensors have been fabricated using a polymer substrate by Kim *et al.* [163]. The design is excellent in achieving flexibility and skin conduction. Using the MEMS technology, the presented bipolar ECG sensors

have been miniaturized whereas, the flexible printed circuit (FPCB) technology has been utilized for the fabrication of polymer-based ECG sensors of the bipolar Laplacian-type electrode. The bipolar ECG sensors have developed for three different sizes of electrodes, i.e., 4 mm, 2 mm, and 1 mm. The fabricated MEMS ECG sensor has two electrodes; a hook-shaped sensing electrode and a reference electrode. The schematic and the optical photograph of the fabricated sensor is given in Fig. 31.

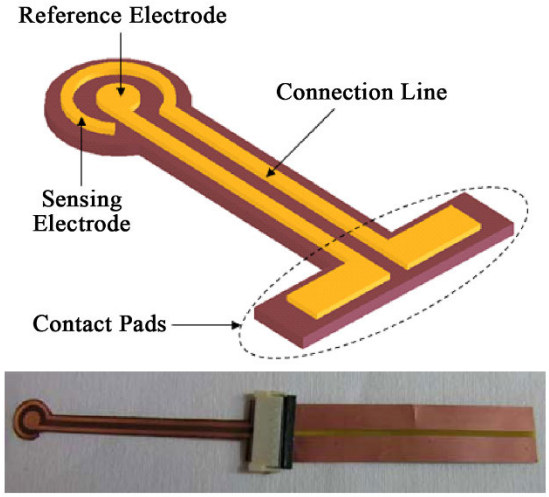

FIGURE 31. The schematic and optical photograph of the fabricated flexible ECG sensor [163].

The ECG measurement capability of the fabricated sensor has also been tested. The ECG of a human is measured using the designed sensor and then compared to a commercially available patch-type ECG electrode. The correlation factor between the two electrodes was 0.977, 0.86, and 0.85 for the 4 mm, 2 mm, and 1 mm electrodes respectively. The results show that the fabricated ECG sensor made by FPCB and MEMS can provide enough information to monitor the condition of the heart and it can be used in implantable devices as well.

A System on Chip (SoC) has been presented by Usman *et al.* [164] which comprises a low frequency, wireless energy harvesting system capable of acquiring, processing, and transmitting ECG along with ballistocardiogram (BCG). An ECG signal is generated due to the electrical activity of the heart and hence, cannot predict any physical blockage well before time. However, the BCG, because it is generated due to the mechanical forces of the heart vessels, can detect any physical blockage earlier than ECG. The presented chip, due to its low-frequency operation and detection, can generate BCG signals as well. Moreover, the designed chip has the capability of autonomous power management and operation using the energy harvesting mechanism.

The proposed design comprises piezoelectric thin film (PZT) elements integrated on top of a silicon beam as-fabricated element. A low resonant frequency is achieved by utilizing the design and arrangement of the proof mass

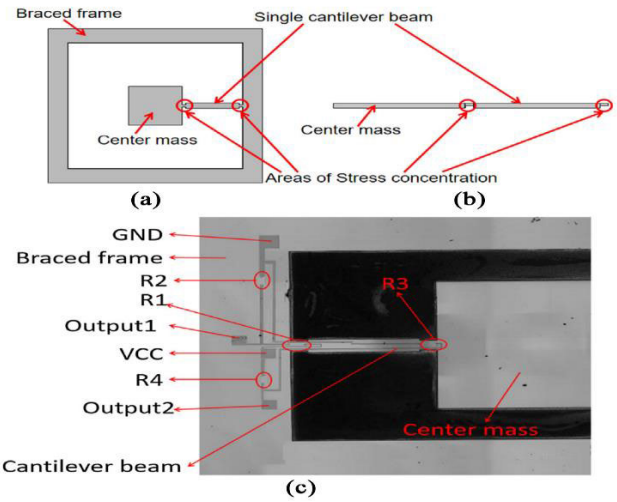

FIGURE 32. Microstructure of a bat-shaped electronic stethoscope sensor (a) top view (b) cross-sectional view (c) fabricated sensor [166].

with the silicon beam. When the proof mass is excited due to any external acceleration, the cantilever undergoes bending. Due to that, a strain is induced at the fixed end of the cantilever. This strain, in turn, induces an electric field in the PZT layer which is extracted with the help of the electrode over the PZT layer. The presented design is capable of ECG extraction and atrial fibrillation detection while consuming only a few μWs of power.

For the continuous monitoring of heart rate in various conditions such as COVID-19, the typically used method needs the attachment of electrodes on the patient's body. The physical attachment of electrodes can sometimes be quite inconvenient, especially from a sleep studies perspective. Hernandez and Cretu [165] have developed and analyzed a single axis MEMS gyroscope based heart rate monitoring system to detect heartbeats, with a -0.3505bpm mean absolute error (MAE) and ± 2.7167bpm standard deviation of the absolute error (SDAE). Due to its small size and low error values, it can be used to monitor heart rate during sleep and detect sustained sinus bradycardias and tachycardias. Moreover, due to its single-axis action, the reported MEMS-heart rate monitor utilizes less power than conventional ECG devices.

To monitor the heart rate, a bat-shaped MEMS electronic stethoscope has been presented by Wang *et al.* [166]. The sensitivity of the presented sensor is measured as 180.7dB at 500Hz with 38dB SNR. The sensor consists of a proof mass and a cantilever beam. The sound signals from the heart can be perceived by the proof mass which causes the cantilever beam to deform. The stress concentration areas on the cantilever beam have piezo-resistors attached. The value of these piezo-resistors changes with the deformation of the stress concentration areas of the cantilever beam. The structure of the stethoscope depicting the cantilever beam mechanism along with the fabricated sensor is given in Fig. 32. To compare the performance of the designed stethoscope with that

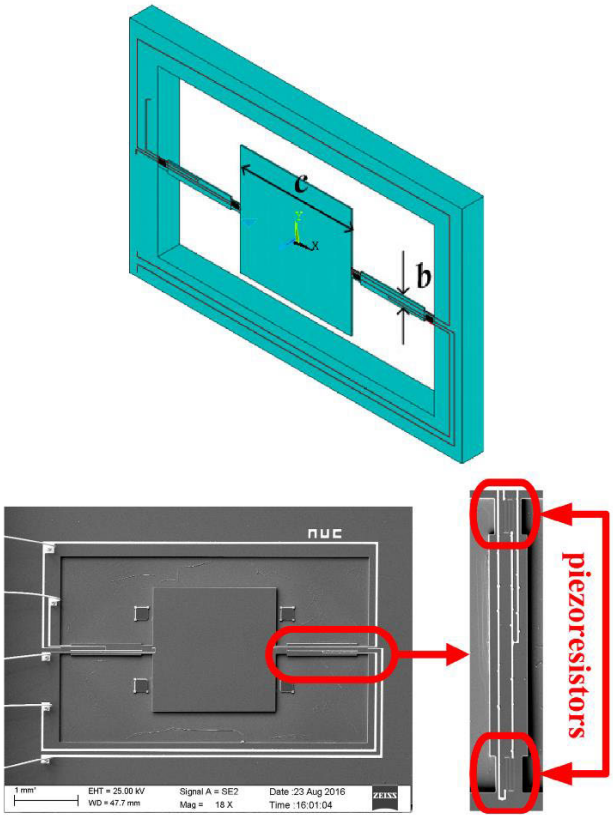

FIGURE 33. Design of the MEMS Piezoresistive electronic heart sound sensor [167].

of a commercial stethoscope, the sound signal of a patient's mitral valve position inside the heart has been captured by both; the designed bat-shaped stethoscope and a 3M (Sau Paulo, MN, USA) electronic stethoscope. The captured signal has been analyzed in the time and frequency domains as well.

The comparison reveals that the signals captured by the presented stethoscope are extremely consistent over a complete sound cycle of the heart. Moreover, the presented MEMS stethoscope provides high sensitivity with a smaller size and easy processing in a measurable bandwidth of 20 Hz to 1 kHz.

A piezoresistive MEMS electronic heart sound sensor is designed and fabricated in [167]. A double-beam-block microstructure is utilized to capture heart sound signals. Structure size is optimized to cater to the frequency response of the heart sound, i.e., 20 to 600 Hz. The double-beam-block MEMS sensor is specifically designed to detect the vibration strength information of the heart sound signal. The designed heart sensor with an SEM image of the fabricated sensor is shown in Fig. 33. For the aforementioned design requirement, the grooves have been placed near the frame and close to the mass block to concentrate the stresses (generated from the detected signal) into the grooves. The piezoresistors are implemented on these grooves to enhance the change rate in the piezo resistors. This helps in detecting the faint heart sounds. For the fabrication of the sensor, a processing technology with the stress concentration grooves has been developed. The fabricated sensor has been tested by comparing the captured sound signal with the commercially available 3M 3200-type electronic stethoscope. The comparison shows that the sound signals captured by the fabricated sensor are the same as that of the commercial stethoscope with a significantly higher signal to noise ratio. Moreover, the presented MEMS sensor also provides the first and second heart sounds providing more information about lesion.

Apart from contact electrodes, development is also being made in noncontact electrodes for ECG. During long-term ECG procedures, contact electrodes may cause allergic reactions, inflammation, and/or metal poisoning as well. A novel non-contact ECG electrode designed using the MEMS process is presented in [168]. To measure a bioelectric signal without directly touching the skin with electrodes, a capacitive coupling mechanism is usually utilized. This mechanism normally utilizes an electrode (made of metal), an insulator, and the skin. These are conjoined together to act as a capacitor that enables the measurement of the signal from the body comfortably. The presented noncontact ECG electrode utilizes this aforementioned capacitive mechanism. It comprises of two conductive plates, an inner and an outer, separated by a thin insulator between them. The inner plate is smaller in size than the outer one and enables the capacitive transduction mechanism. The bio-potential variations on the skin generate a voltage signal which is further conditioned by a signal conditioning circuit board. The outer plate, on the other hand, is used for the purpose of shielding, i.e., to protect the inner plate from external electromagnetic noise. Furthermore, for noise reduction, the lead wires of the electrode are designed coaxially to prevent the cables from coupling to the ground or electronic device. The design of the non-contact electrode and the fabricated electrode is shown in Fig. 34. The developed prototype electrode has an area of about 2.324 cm^2. The electrode has been tested on a 26-year-old subject and results have been verified and compared with an ECG simulator. The recorded signals are comparable to those of the ECG simulator. The developed prototype ECG electrode can measure ECG at 500 μm distance from the subject's chest. Moreover, it is flexible, passive, biocompatible, and capable of eliminating environmental electromagnetic interferences.

III. DISCUSSION

The severity of the COVID-19 situation is increasing steadily, and it has been quite difficult to control. Countries are applying different tactics to control the virus spread within their communities. In response, various feasible treatment methods have been employed, and some are in progress. Severely affected but economically stable countries such as the USA, Italy, Germany, etc. have managed to provide critical healthcare to affected citizens, but low-economic status nations have been unable to do so due to fewer health facilities and less available equipment. The need of the hour is the

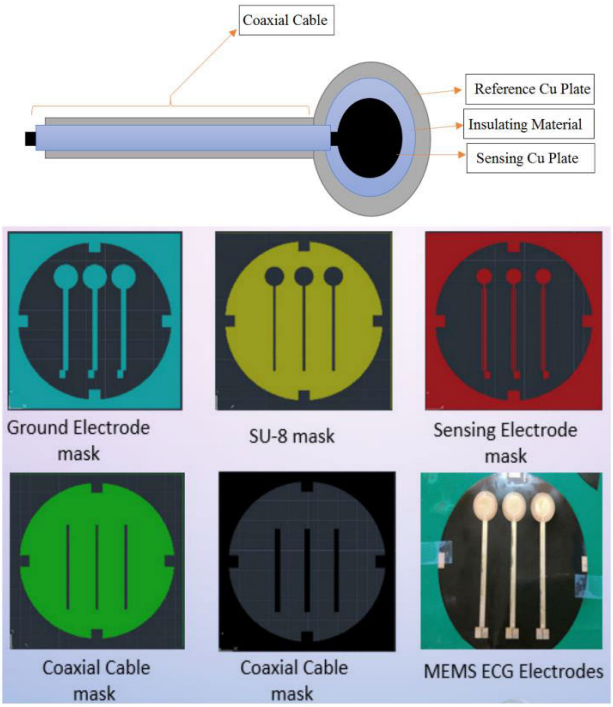

FIGURE 34. Design of the noncontact ECG electrode with photomasks and fabricated electrode [168].

availability of low-cost but highly precise devices/equipment, and the performance and precision of the equipment is dependent on the sensors used. This article reviews various designs and working principles of MEMS sensors involved in the equipment used for the treatment of COVID-19, which is also a limitation of this study, i.e., it only presents sensors that have been reported in context of applications related to the equipment used in the treatment of COVID-19 or proposed for biomedical applications related to the equipment. In other words, a large number of MEMS pressure sensors can be found in literature, but here, only those reported to be used in and that could be used in equipment like ventilators, pulse oximeters, syringe pumps, patient monitors, etc. are examined and reviewed. The comparison was performed on the basis of the operating principle/mechanism, performance parameters (sensitivity, operating range, SNR, etc.) and applications of the reported sensors. Furthermore, the review presented in this article focuses not only on existing/commercially available MEMS sensors but also sensors that have been proposed in the research literature for similar applications. Therefore, a key purpose of this study is to help future researchers by summarizing the published literature concerning applications involving five major equipment types, i.e., ventilators, pulse oximeter, syringe/infusion pump, patient monitor and ECG, and help them find research gaps in the aforementioned applications/equipment. The sensors reviewed in Section II are discussed here, and a summary of all reviewed sensors is given in Table V.

In a common ventilator, the sensors may be categorized into two main types: flow sensors and pressure sensors. Flow sensors are used to measure air/gas flow into and out of the patient's lungs or to monitor bidirectional flow for unexpected flow reversal. The design and working principles of various types of flow sensors, e.g., thermal, non-thermal, piezo-resistive, liquid crystal polymer, calorimetric thermal flow sensors, biomimetic flow sensors, etc., and some commercially available high-performance sensors, such as Sensirion single-use MEMS sensors, have been reviewed. Among thermal flow sensors, the thermal convection mechanism is utilized in the majority of the reported sensors and has very fast response times. Although thermal flow sensors are the most preferred sensors for the measurement of direction and velocity in certain biomedical applications, their application is normally limited to non-corrosive environments. They require special packaging to avoid degradation [126]. Moreover, polysilicon thermopile sensors also prove to be a viable option, with a detection range of 0-50 m/s, and the use of polysilicon makes these sensors easy to manufacture. Furthermore, Sensirion single-use MEMS flow sensors are autocalibrated and do not need to be sterilized, making them suitable for use in modern ventilators, especially during a pandemic, when there is no time to calibrate or sterilize the sensors with hundreds of patients needing ventilation at the same time. These sensors provide a fully calibrated and temperature-compensated output signal. Such sensors hold remarkable importance in future portable equipment and are likely to dominate the sensor market. A concern of greater importance associated with commercializing MEMS flow sensors for biomedical applications, especially for invasive applications, is that polymer (soft) materials should be used for sensing elements and structures. Although polymer-based sensors hold high market value, most commercially available sensors are silicon-based. The possible roadblocks causing polymer-based sensors to not be preferred for biomedical applications are parameters such as the response time, repeatability and accuracy, which still need to be explored. A summary of the reviewed flow sensors is presented in Table V.

The pressure sensors used in a ventilator have also been discussed. MEMS pressure sensors reduce ventilator-associated and -induced lung injuries, i.e., VALI and VILI, which are most common in ventilators with conventional sensors. The majority of recently developed MEMS pressure sensors are capacitive pressure sensors. In capacitive pressure sensors, the differential capacitance mechanism with a diaphragm deflection method is the most reported operating mechanism, and in the diaphragm design procedures for pressure sensors, it has been shown that thicker perforated diaphragms provide better sensitivities than thinner nonperforated diaphragms. Among diaphragm deflection mechanism sensors, very low-pressure sensitivity is achieved using a CMOS capacitive pressure sensor with a maximum detectable pressure of 500 hPa. Among all available MEMS pressure sensors for biomedical applications, piezoresistive pressure sensors are still widely used due their high yield, wide dynamic range and linear operation over a

considerable range of pressures. However, the efficiency of MEMS pressure sensors is highly dependent on temperature and humidity, especially in biomedical applications [169]. For this reason, capacitive MEMS pressure sensors are gaining importance, and this importance also accounts for the recent development of capacitive MEMS pressure sensors focusing on lower temperature sensitivity. A summary of the reported pressure sensors in the context of ventilators can be seen in Table V.

In the context of pulse oximeters, various sensors for the measurement of oxygen saturation, the respiration rate, pulse waves or the heart rate have been presented. Most recently reported oxygen saturation sensors are implantable and are moving towards wearable technology. Wearable technology holds great importance in future epidemics and pandemics [170]. Due to the development of small size and low powered devices, wearable devices having multiple sensors that can monitor symptoms of a patient, store data, and can also provide access to medical personnel are available these days and such devices will be quite common in the future [170]. An important issue that needs attention in the development of the latest oxygen saturation measurement sensors is the long-term monitoring of oxygen. This issue has been addressed and resolved in [145]. A MEMS biocompatible oxygen sensor has been designed and tested to resolve the issue of long-term monitoring of oxygen. The designed sensor uses an electrochemical mechanism, and electrical signals are collected from analyte reactions. The integration of such sensors into the newest/future pulse oximeters can help in monitoring critically ill patients, e.g., for conditions such as chronic respiratory failure. Furthermore, to improve the spatial resolution of respiration monitoring sensors, the use of magnetic sensors with a magnetic field variation mechanism has been investigated. This resulted in a high spatial resolution, which is an important parameter in respiration monitoring. For pulse wave measurements, the most utilized MEMS mechanism is the differential pressure mechanism. The newest pulse oximeters with MEMS sensors are rapidly replacing conventional bulky oximeters, especially in wearables. With the increasing importance of implantable medical electronics and wearables, the main challenge in their development is extending the lifespan of such devices. Commendable development of MEMS energy harvesters has been achieved to make these devices self-powered. These devices are made self-powered by utilizing in vivo energy harvesting and charging by making use of the body movements and internal physiological environment. In this regard, various techniques of energy conversion for in vivo thermal, mechanical, and chemical sources have been reported. Of these reported sources, mechanical energy-based harvesters are the most popular and highly recommended. These harvesters convert the minute mechanical movements inside the human body into electric energy. Mechanical energy harvesting in MEMS energy harvesters is usually achieved by electromagnetic interactions, electrostatic induction (triboelectric harvesting) and piezoelectric effects. For implantable devices and other related biomedical applications, piezoelectric energy harvesters are the most suitable candidates for capturing and converting biomechanical energy into electric energy [171]. Moreover, recent advancements in the development of piezoelectric nanogenerators (PENGs) have allowed these ideal candidates to be used in implantable biomedical devices. Thus, PENGs have a promising future in powering implantable and wearable materials [171], [172]. Recently reported piezoelectric nanogenerators can provide commendable output voltages, e.g., 1 V at 2 Hz vibrations [173] and 1.1 V with a 2 μA peak current [174]. These outputs are quite promising for powering autonomous sensors in the μW-mW range. A summary of MEMS sensors for pulse oximeters is given in Table V.

The sensors in syringe/infusion pumps have been categorized as force sensors and pressure sensors. Among the presented commercially available force sensors, the Honeywell RSS series shows promising benefits. These sensors work on the low deflection principle, which is approx. 30 μm at full scale. This helps in the reduction of measurement errors. Furthermore, the sensor output of the RSS series has low sensitivity to many mounting stresses, giving precise and steady output even at low forces. For the measurement of ultralow forces, a PDMS MEMS sensor that utilizes a piezoresistive microcantilever-based sensing mechanism has been reported. It can measure forces in a range of 0-100 μN and offers a sensitivity of 0.6712 mV/V/μN.

Commercially available pressure sensors for the application of infusion pumps have been discussed and compared. The TruStability^{TM} series offers decent and reliable sensors with a pressure range of $\pm$160 Pa to $\pm$1 MPa. A piezoresistive silicon pressure transducer is utilized in these sensors. These sensors are widely used in commercially available infusion pumps and anaesthesia machines. Moreover, for low pressures and sensitivity enhancement, a graphene piezoresistive MEMS pressure sensor was reported in [155]. Due to enhanced sensitivity and increased temperature capability, sensors utilizing graphene holds incredible importance in terms of future market coverage and multiple applications in future biomedical equipment.

In a patient monitor, blood pressure measurement and temperature measurement sensors are of significant importance. For blood pressure measurement, the important parameters in considering sensors are continuous monitoring and, most preferably, noninvasive measurement. Sensors reported for both aforementioned purposes mostly utilize the capacitive mechanism. A capacitive MEMS pressure sensor is reported [157] for continuous monitoring of blood pressure, utilizing the diaphragm deflection mechanism with a 0-0.16 MPa pressure range and a sensitivity of 7.97 fF/bar. However, along with continuous monitoring, high sensitivity is also an indispensable property. To improve the sensitivity of blood pressure measurement, the piezoresistive diaphragm mechanism is utilized in [158]. This novel sensor based on temporary bonding technology needs attention from

TABLE 5. Summary of the mems sensors for the equipment used in COVID-19 treatment.

MEMS Sensor Type	Parameter	Operating Principle/ Mechanism	Purpose/ Application
Ventilators (Flow Sensors)			
Impaltable Catheter flow sensor [119]	Response time: 0.23s Detectable Breathing Freq. Range: 0.63 Hz to 1.9 Hz	Hot-wire Anemometry	Breathing characteristics measurement.
Tube-type thermal flow sensor [120]	N.A.	Thermal convection.	- Positive pressure airflow measurement. - Evaluate lung's elasticity
Micro-Hair Polymer flow sensor [121]	Min. velocity Sensing: 0.66 to 0.97 m/s Sensitivity: 123 mV/(m/s)$^{-1}$	Conductive polymers.	Ultra low airflow velocity measurement.
Thermal gas flow sensor [122]	Response Time: 250ms	Thermal convection.	Gas flow measurement.
Sensirion single use flow sensors (SFM3300) [85]	Sensitivity: 250 l/min (bidirectional)	- Patented MEMS mechanisms - CMOSens® chips	- Respiration monitoring (bidirectional). - In ventilator/anesthesia machine.
Thermal flow sensors [105]	Sensitivity: 0.05 l/min	Converts heat transfer of fluid flow into electrical signals.	Flow rate measurement.
Non-thermal flow sensors [106-110]	Detection Range: 0.01 to 45 m/s	deflection of the cantilever, differential pressure, etc.	Flow sensing.
Piezoresistive flow sensor [103]	Sensitivity: 7.4 µl/min	Piezoresistive cantilevers.	Fluid flow detection.
Liquid Crystal Polymer flow sensor [123]	Sensitivity: 33.33 µl/min	Polymer Strain Gauge.	Intravenous infusion rate measurement.
Biomimetic MEMS flow sensor [127]	Sensing range: 0 to 0.7 m/s	Biomemtic Cupula Structure.	Steady state and oscillatory flow measurement.
Calorimetric thermal flow sensors [115]	Sensitivity: 100 ml/min	Converts heat transfer of fluid flow into electrical signals.	Flow rate measurement.
Ventilators (Pressure Sensors)			
Silicon Piezoresistive Pressure Sensor [79]	Max Detectable Pressure: 20 KPa	- Differential pressure. - Meso channel integrated with a pressure sensor.	Measure Oxygen flow in a pediatric ventilator
Capacitive Pressure Sensor [130]	Max Detectable Pressure: 30 KPa	- Silicon diaphragm bending. - Differential Capacitance	- Heart rate detection. - Radial artery pulse measurement.
Monolithically fabricated Capacitive pressure sensor [131]	Max Detectable Pressure: 8 KPa	- Top plate deflection. - Change in Capacitance.	Cardiological Applications
CMOS Capacitive pressure sensor [132]	Max Detectable Pressure: 500 hPa Sensitivity: 8.72 mV/V/hPa	- Diaphragm deflection. - Change in capacitance.	Low-pressure measurement, e.g., arterial, intraocular, etc.
Pulse Oximeter			
Micromachined Optical sensor [144]	Sampling Rate: 200 Hz	Light absorption	Oxygen saturation measurement.
MEMS magnetic sensor [146]	Sampling Rate: 250 Hz	Magnetic Field variation	Respiration monitoring
A wearable array of pressure sensors (SCB10H) [130]	Sensitivity: 55 fF/kPa	Capacitive absolute pressure sensing (Diaphragm bending)	- Radial artery pulse wave measurement. - Heart rate detection.
MEMS piezoresistive cantilever Pulse wave sensor [147]	Sampling Rate: 400 Hz	Differential pressure measurement	Pulse wave velocity
MEMS piezoresistive cantilever pressure sensor [148]	Sampling Rate: 100 Hz	Differential air pressure measurement	- Respiratory rate - Pulse rate
MEMS biocompatible oxygen sensor [145]	Sampling Rate: 10 – 100 MHz	- Electrochemical - Measurement of the electrical signal from analyte reactions.	- Oxygen Saturation Measurement. - Long-term oxygen monitoring
Syringe/Infusion Pump (Force Sensors)			
Honeywell FSS, FSG, FSS-SMT series [151]	Sensitivity: 6.6 mV/V/N Force Sensing Range: 0 – 5 N	Solid-state Piezoresistive pressure transducer.	Force sensing in infusion pumps.

TABLE 5. ***(continued)*** **Summary of the mems sensors for the equipment used in COVID-19 treatment.**

Amorphous carbon film MEMS force sensor [152]	Sensitivity: 80.7 µV/V/N Force Sensing Range: 0–1.16 N	Piezoresistive pressure transducer	Low force sensing.
PDMS MEMS force sensor [153]	Sensitivity: 1.62 mV/µN Force Sensing Range: 0-100 µN	Piezoresistive sensing mechanism.	Low magnitude forces.
	Syringe/Infusion Pump (Pressure Sensors)		
TruStability RSC series [151]	Pressure Range: ±160Pa to ±1 MPa	Piezoresistive silicon pressure transducer.	Airflow monitors, anesthesia machines, etc.
TruStability HSC, SSC series [151]	Pressure Range: ±160 Pa to ±1 MPa	Piezoresistive silicon pressure transducer.	Airflow monitors, anesthesia machines, etc.
Piezo-resistive pressure sensor based on Carbon Nanotubes [154]	Sensitivity: 95.5 kPa^{-1} Sensing threshold: 16 Pa	- PDMS Electrodes - Carbon nanotubes.	Ultra-low pressure sensing for wearables, biomedical equipment.
Graphene Piezoresistive MEMS pressure sensor [155]	Sensitivity: 3.98 mV/psi	Graphene piezoresistive pressure transducer.	Low-pressure applications.
	Patient Monitor		
MEMS Piezoelectric Cantilever Blood Pressure Sensor [156]	Pressure Range: 8 - 24KPa Max. deflection: 4.95µm	Piezoelectric cantilever deflection.	Non-invasive blood pressure measurement.
Capacitive MEMS Pressure Sensor [157]	Pressure Range: 0–0.16 MPa Sensitivity: 7.97 fF/bar	Diaphragm deflection.	Continuous blood pressure measurement.
Piezoresistive MEMS Pressure Sensors [158]	Pressure Range: 0 – 180 kPa Sensitivity: 36µV/(V.kPa)	Piezoresistive diaphragm.	Blood pressure measurement
MEMS Resonator based Thermometer SoC [159]	Temperature Range: -40 to 120 ^{0}C	MEMS resonator	Temperature measurement.
MEMS resonator-based thermometer with RTC [160]	Temperature Range: 0 to 100 ^{0}C Sensitivity: -5.7 Hz/ ^{O}C or 0.224 mV/^{O}C	MEMS resonator.	Temperature compensation for stable temperature response.
MEMS thermometer on flexible polyamide [161]	Temperature Range: 25 – 200 ^{o}C	Resistance variation.	Temperature measurement.
	ECG		
Microneedles based electrode [162]	Microneedle depth: 100µm Microneedle diameter: 100µm	Potential difference due to ionic concentration	ECG measurement.
Bipolar-Laplacian type Flexible ECG electrode [163]	Electrode diameter: 4 mm Correlation Factor: 0.977	Potential difference b/w sensing electrode and reference electrode.	ECG measurement.
MEMS energy harvesting SoC [164]	Low-frequency range: 1-50 Hz	Piezo-electric cantilever deflection.	ECG and BCG measurement.
Piezoresistive electronic stethoscope [166]	SNR: 32 dB Bandwidth: 20Hz to 1kHz	Piezoresistive.	- Monitoring heartbeats. - Heart rate measurement.
MEMS Gyroscope [165]	Mean Absolute Error: -0.3505 bpm. Standard Deviation of Absolute Error: ±2.7 bpm.	Angular rate data and acceleration detection.	- Heart rate measurement. - Heartbeat detection.
Piezoresistive Electronic Heart Sound Sensor [167]	SNR: 27 dB SNR Bandwidth: 20 to 600 Hz.	Piezoresistive.	Heart sound sensor.
Noncontact ECG Electrode [168]	ECG amplitude: 1.5 V Non-contact distance: 500 µm	Capacitive coupling mechanism.	- Noncontact ECG measurement.

manufacturers for use in highly sensitive patient monitoring applications, as it exhibits a sensitivity of 36 μV/(V.kPa).

Resistance variation is the most commonly used mechanism in MEMS temperature sensors. However, MEMS resonator-based thermometers are now gaining more attention from designers and are designed such that a suspended mass resonates at different temperature values. This mechanism gives precise temperature measurements among MEMS temperature measurement devices. The temperature range of one such reported sensor is -40 to 120 °C. These sensors prove to be a good option for application in patient monitoring. A summary of the sensors used in patient monitors is given in Table V.

The contribution of MEMS technology to applications in electrocardiograms (ECGs) mainly revolves around the development of different types of new electrodes. These new electrodes should have the following important characteristics: 1) they should exclude painful preparatory procedures such as applying gel, 2) they should resolve issues arising due to high electrode-skin-electrode impedance (ESEI), and 3) they should be small in size, flexible and biocompatible. A MEMS microneedle-based electrode developed in [162] offers much lower electrode-skin-electrode impedance by measuring the potential difference due to the ionic concentration in the microneedles. For future devices, especially portable and/or wearable devices, wireless data acquisition is very important. In addition to wireless data acquisition, noncontact ECG electrode development is a focus for future devices because contact electrodes may pose threats such as inflammation, metal poisoning, and/or allergic reactions during long-term ECG procedures. Although the development of such electrodes is not new and dates back a few decades, it has recently received more attention. Such a noncontact ECG electrode has been developed recently [168] by utilizing a capacitive coupling mechanism. Several other small and wearable electrodes have also been reported. Standard electrodes are rapidly being exchanged for these new microstructure electrodes, as these electrodes tend to be flexible, biocompatible, and less painful and remove the need for preparatory procedures involving gels and medicines [162]. A summary of the electrodes used for ECG measurement is given in Table V.

This article primarily focuses on the role of MEMS sensors in the fight against present and future pandemics. A salient perspective to be focused upon is that such pandemics require rapid transport solutions to ensure availability of the requisite equipment in all countries. In comparison to equipment using conventional sensors, equipment incorporating MEMS sensors has higher portability due to the corresponding reduction in size and weight and, hence, can easily be transported anywhere. In addition, MEMS/NEMS sensors are highly biocompatible for use inside the patient body, i.e., in vivo applications for regular monitoring of basic vitals. Other indispensable factors that make MEMS-based sensors and devices preferable over conventional sensors for biomedical applications are reusability and sterilization. The reusability of conventional sensors requires proper sterilization, and there are chances of disease transmission. MEMS sensors rule out these issues, as they tend to be portable and disposable. Due to their small size and low manufacturing cost, instead of reuse, MEMS sensors can be replaced with a new sensor for each use, which ends the need for sterilization.

Another important perspective realizing the significance of MEMS in the fight against such pandemics is that during such emergencies, which tend to prevail for a long duration, with the number of patients increasing exponentially, there should be adequate local facilities for research, development, and manufacturing of microsensors/actuators. The unavailability of such facilities, especially in lower-middle-economic status countries (to one of which the authors belong), is one of the major reasons behind low recovery rates and uncontrolled increases in the number of deaths. Such countries solely depend on the import of such equipment, which, in these situations, is delayed. Focusing on indigenous research and development of MEMS technology and manufacturing facilities can facilitate quick diagnoses and avoid a large number of casualties in such pandemics, especially in the future, due to the availability of local, low-cost and precise equipment. Therefore, a key purpose of the article is to highlight the importance of MEMS sensors in situations such as the current pandemic and to attract the focus of the local industry/academia to establish microfabrication facilities in lower-middle-economic status countries. The establishment of microfabrication facilities will help bridge the gap between industry and academia.

IV. CONCLUSION

This study highlights the role and advancement of MEMS technology in the improvement of conventional equipment used in biomedical and health care applications. The ongoing miniaturization of the sensors and actuators has helped in the cost reduction of the equipment. Also, the progressing research on MEMS sensors has resulted in more accurate sensors and actuators especially for micro and nanoscale measurements. Due to the desired size reduction, precision enhancement, and ease in circuit integration, very minute measurements in invasive applications have also been made easier. The devices/sensors reviewed in this article throw light on the inevitable importance of MEMS sensors in current healthcare equipment used in the treatment of COVID19, depicting how rapidly they have replaced conventional sensors and can revolutionize the future equipment due to their portability, enhanced performance, low-cost manufacturing, and easy integration.

REFERENCES

[1] H. Lu, C. W. Stratton, and Y. W. Tang, "Outbreak of pneumonia of unknown etiology in Wuhan, China: The mystery and the miracle," *J. Med. Virol.*, vol. 92, no. 4, pp. 401–402, Apr. 2020, doi: 10.1002/jmv.25678.

[2] Q. Li, X. Guan, P. Wu, X. Wang, and L. Zhou, "Early transmission dynamics in Wuhan, China, of novel coronavirus–infected pneumonia," *New England J. Med.*, vol. 382, no. 13, pp. 1199–1207, Mar. 2020, doi: 10.1056/NEJMoa2001316.

[3] E. Mahase, "China coronavirus: WHO declares international emergency as death toll exceeds 200," *BMJ*, vol. 368, p. m408, Jan. 2020, doi: 10.1136/bmj.m408.

[4] World Health Organization, COVID-19 Weekly Epidemiological Update. Geneva, Switzerland: WHO, 2020.

[5] S. Law, A. W. Leung, and C. Xu, "Severe acute respiratory syndrome (SARS) and coronavirus disease-2019 (COVID-19): From causes to preventions in hong kong," *Int. J. Infectious Diseases*, vol. 94, pp. 156–163, May 2020, doi: 10.1016/j.ijid.2020.03.059.

[6] A. Zumla, D. S. Hui, and S. Perlman, "Middle East respiratory syndrome," *Lancet*, vol. 386, no. 9997, pp. 995–1007, Mar. 2015, doi: 10.1016/S0140-6736(15)60454-8.

[7] World Health Organization, *MERS Situation Update*, WHO, Geneva, Switzerland, Dec. 2019.

[8] J. Cui, F. Li, and Z.-L. Shi, "Origin and evolution of pathogenic coronaviruses," *Nature Rev. Microbiol.*, vol. 17, no. 3, pp. 181–192, Mar. 2019, doi: 10.1038/s41579-018-0118-9.

[9] C.-C. Lai, T.-P. Shih, W.-C. Ko, H.-J. Tang, and P.-R. Hsueh, "Severe acute respiratory syndrome coronavirus 2 (SARS-CoV-2) and coronavirus disease-2019 (COVID-19): The epidemic and the challenges," *Int. J. Antimicrobial Agents*, vol. 55, no. 3, Mar. 2020, Art. no. 105924, doi: 10.1016/j.ijantimicag.2020.105924.

[10] World Health Organization, *Laboratory Testing for Coronavirus Disease 2019 (COVID-19) in Suspected Human Cases: Interim Guidance*, WHO, Geneva, Switzerland, Mar. 2020.

[11] M. A. Shereen, S. Khan, A. Kazmi, N. Bashir, and R. Siddique, "COVID-19 infection: Origin, transmission, and characteristics of human coronaviruses," *J. Adv. Res.*, vol. 24, pp. 91–98, Jul. 2020, doi: 10.1016/j.jare.2020.03.005.

[12] N. Chen, M. Zhou, X. Dong, J. Qu, F. Gong, Y. Han, and Y. Qiu, "Epidemiological and clinical characteristics of 99 cases of 2019 novel coronavirus pneumonia in Wuhan, China: A descriptive study," *Lancet*, vol. 395, no. 10223, pp. 507–513, May 2020, doi: 10.1016/S0140-6736(20)30211-7.

[13] D. Wang, B. Hu, C. Hu, F. Zhu, X. Liu, J. Zhang, and B. Wang, "Clinical characteristics of 138 hospitalized patients with 2019 novel coronavirus–infected pneumonia in Wuhan, China," *JAMA*, vol. 323, no. 11, pp. 1061–1069, Feb. 2020, doi: 10.1001/jama.2020.1585.

[14] R. Lu, X. Zhao, J. Li, P. Niu, B. Yang, H. Wu, and W. Wang, "Genomic characterisation and epidemiology of 2019 novel coronavirus: Implications for virus origins and receptor binding," *Lancet*, vol. 395, no. 10224, pp. 565–574, Feb. 2020.

[15] P. Zhou, X. L. Yang, X. G. Wang, B. Hu, L. Zhang, and W. Zhang, "A pneumonia outbreak associated with a new coronavirus of probable bat origin," *Nature*, vol. 579, no. 7798, pp. 270–273, Mar. 2020.

[16] W. B. Yu, G. D. Tang, L. Zhang, and R. T. Corlett, "Decoding the evolution and transmissions of the novel pneumonia coronavirus (SARS-CoV-2/HCoV-19) using whole genomic data," *Zool. Res.*, vol. 41, no. 3, pp. 247–257, Mar. 2020.

[17] Y. Bai, L. Yao, T. Wei, F. Tian, D. Y. Jin, L. Chen, and M. Wang, "Presumed asymptomatic carrier transmission of COVID-19," *JAMA*, vol. 323, no. 14, pp. 1406–1407, Aug. 2020, doi: 10.1001/jama.2020.2565.

[18] NHS. (2020). *National Health Commission (NHC) of the People's Republic of China*, [Online]. Available: http://en.nhc.gov.cn/

[19] World Health Organization, *Coronavirus Disease (COVID-19) Weekly Epidemiological Update*, WHO, Geneva, Switzerland, 2020.

[20] F. Gentile, A. Aimo, F. Forfori, G. Catapano, A. Clemente, F. Cademartiri, M. Emdin, and A. Giannoni, "COVID-19 and risk of pulmonary fibrosis: The importance of planning ahead," *Eur. J. Preventive Cardiol.*, vol. 27, no. 13, pp. 1442–1446, Sep. 2020, doi: 10.1177/2047487320932695.

[21] D. J. Bell and H. Knipe. (2020). *COVID-19*. [Online]. Available: https://radiopaedia.org/articles/covid-19-4

[22] W. Yang, Q. Cao, L. E. Qin, X. Wang, Z. Cheng, and A. Pan, "Clinical characteristics and imaging manifestations of the 2019 novel coronavirus disease (COVID-19): A multi-center study in Wenzhou city, Zhejiang, China," *J. Infection*, vol. 80, no. 4, pp. 388–393, Apr. 2020, doi: 10.1016/j.jinf.2020.02.016.

[23] R.-F. Chen, J.-C. Chang, W.-T. Yeh, C.-H. Lee, J.-W. Liu, H.-L. Eng, and K. D. Yang, "Role of vascular cell adhesion molecules and leukocyte apoptosis in the lymphopenia and thrombocytopenia of patients with severe acute respiratory syndrome (SARS)," *Microbes Infection*, vol. 8, no. 1, pp. 122–127, Jan. 2006, doi: 10.1016/j.micinf.2005.06.007.

[24] W. G. Carlos, C. S. D. Cruz, B. Cao, S. Pasnick, and S. Jamil, "COVID-19 disease due to SARS-CoV-2 (novel coronavirus)," *Amer. J. Respiratory Crit. Care Med.*, vol. 201, no. 4, pp. P7—8, May 2020, doi: 10.1164/rccm.2014P7.

[25] W. Wang, J. Tang, and F. Wei, "Updated understanding of the outbreak of 2019 novel coronavirus (2019-nCoV) in Wuhan, China," *J. Med. Virol.*, vol. 92, no. 4, pp. 441–447, Feb. 2020, doi: 10.1002/jmv.25689.

[26] C. Huang, Y. Wang, X. Li, L. Ren, J. Zhao, Y. Hu, and L. Zhang, "Clinical features of patients infected with 2019 novel coronavirus in Wuhan, China," *Lancet*, vol. 395, no. 10223, pp. 497–506, Jun. 2020, doi: 10.1016/S0140-6736(20)30183-5.

[27] X. Li, M. Geng, Y. Peng, L. Meng, and S. Lu, "Molecular immune pathogenesis and diagnosis of COVID-19," *J. Pharmaceutical Anal.*, vol. 10, no. 2, pp. 102–108, Apr. 2020, doi: 10.1016/j.jpha.2020.03.001.

[28] M. Wang, R. Cao, L. Zhang, X. Yang, J. Liu, M. Xu, Z. Shi, Z. Hu, W. Zhong, and G. Xiao, "Remdesivir and chloroquine effectively inhibit the recently emerged novel coronavirus (2019-nCoV) in vitro," *Cell Res.*, vol. 30, no. 3, pp. 269–271, Feb. 2020, doi: 10.1038/s41422-020-0282-0.

[29] M. L. Agostini, A. J. Pruijssers, and J. D. Chappell, "Small-molecule antiviral β-d-N4-hydroxycytidine inhibits a proofreading-intact coronavirus with a high genetic barrier to resistance," *J. Virol.*, vol. 93, no. 24, Jun. 2019, Art. no. e01348, doi: 10.1128/JVI.01348-19.

[30] H. Lu, "Drug treatment options for the 2019-new coronavirus (2019-nCoV)," *Biosci. Trends*, vol. 14, no. 1, pp. 69–71, Feb. 2020, doi: 10.5582/bst.2020.01020.

[31] T. P. Sheahan, A. C. Sims, S. R. Leist, A. Schäfer, J. Won, A. J. Brown, S. A. Montgomery, A. Hogg, D. Babusis, M. O. Clarke, J. E. Spahn, L. Bauer, S. Sellers, D. Porter, J. Y. Feng, T. Cihlar, R. Jordan, M. R. Denison, and R. S. Baric, "Comparative therapeutic efficacy of remdesivir and combination lopinavir, ritonavir, and interferon beta against MERS-CoV," *Nature Commun.*, vol. 11, no. 1, pp. 1–14, Dec. 2020, doi: 10.1038/s41467-019-13940-6.

[32] J. S. Morse, T. Lalonde, S. Xu, and W. R. Liu, "Learning from the past: Possible urgent prevention and treatment options for severe acute respiratory infections caused by 2019-nCoV," *Chembiochem*, vol. 21, no. 5, pp. 730–738, Mar. 2020, doi: 10.1002/cbic.202000047.

[33] J. Gao, Z. Tian, and X. Yang, "Breakthrough: Chloroquine phosphate has shown apparent efficacy in treatment of COVID-19 associated pneumonia in clinical studies," *Biosci. Trends*, vol. 14, no. 1, pp. 72–73, Feb. 2020, doi: 10.5582/bst.2020.01047.

[34] J. Mair-Jenkins, M. Saavedra-Campos, J. K. Baillie, P. Cleary, F.-M. Khaw, W. S. Lim, S. Makki, K. D. Rooney, J. S. Nguyen-Van-Tam, C. R. Beck, and C. Plasma Study Group, "The effectiveness of convalescent plasma and hyperimmune immunoglobulin for the treatment of severe acute respiratory infections of viral etiology: A systematic review and exploratory meta-analysis," *J. Infectious Diseases*, vol. 211, no. 1, pp. 80–90, Jan. 2015, doi: 10.1093/infdis/jiu396.

[35] M. Xie and Q. Chen, "Insight into 2019 novel coronavirus–An updated interim review and lessons from SARS-CoV and MERS-CoV," *Int. J. Infectious Diseases*, vol. 94, pp. 119–124, May 2020, doi: 10.1016/j.ijid.2020.03.071.

[36] C. Shen, Z. Wang, F. Zhao, Y. Yang, J. Li, J. Yuan, and F. Wang, "Treatment of 5 critically ill patients with COVID-19 with convalescent plasma," *JAMA*, vol. 323, no. 16, pp. 1582–1589, Oct. 2020, doi: 10.1001/jama.2020.4783.

[37] H. Weingartl, M. Czub, S. Czub, and J. Neufeld, "Immunization with modified vaccinia virus ankara-based recombinant vaccine against severe acute respiratory syndrome is associated with enhanced hepatitis in ferrets," *J. Virol.*, vol. 78, no. 22, pp. 12672–12676, Nov. 2004, doi: 10.1128/JVI.78.22.12672-12676.2004.

[38] J. Corum, D. Grady, S. L. Wee, and C. Zimmer. (2020). *Coronavirus Vaccine Tracker*. [Online]. Available: https://www.nytimes.com/interactive/2020/science/coronavirus-vaccine-tracker.html

[39] H. Bisht, A. Roberts, L. Vogel, K. Subbarao, and B. Moss, "Neutralizing antibody and protective immunity to SARS coronavirus infection of mice induced by a soluble recombinant polypeptide containing an N-terminal segment of the spike glycoprotein," *Virology*, vol. 334, no. 2, pp. 160–165, Apr. 2005, doi: 10.1016/j.virol.2005.01.042.

[40] Y. W. Kam, F. Kien, A. Roberts, and Y. C. Cheung, "Antibodies against trimeric S glycoprotein protect hamsters against SARS-CoV challenge despite their capacity to mediate FcγRII-dependent entry into B cells *in vitro*," *Vaccine*, vol. 25, no. 4, pp. 729–740, Jun. 2007, doi: 10.1016/j.vaccine.2006.08.011.

[41] Z.-Y. Yang, W.-P. Kong, Y. Huang, A. Roberts, B. R. Murphy, K. Subbarao, and G. J. Nabel, "A DNA vaccine induces SARS coronavirus neutralization and protective immunity in mice," *Nature*, vol. 428, no. 6982, pp. 561–564, Apr. 2004, doi: 10.1038/nature02463.
[42] K. Stadler, A. Roberts, S. Becker, L. Vogel, M. Eickmann, L. Kolesnikova, H.-D. Klenk, B. Murphy, R. Rappuoli, S. Abrignani, and K. Subbarao, "SARS vaccine protective in mice," *Emerg. Infectious Diseases*, vol. 11, no. 8, pp. 1312–1314, Aug. 2005, doi: 10.3201/eid1108.041003.
[43] S. U. Kapadia, J. K. Rose, E. Lamirande, L. Vogel, K. Subbarao, and A. Roberts, "Long-term protection from SARS coronavirus infection conferred by a single immunization with an attenuated VSV-based vaccine," *Virology*, vol. 340, no. 2, pp. 174–182, Sep. 2005, doi: 10.1016/j.virol.2005.06.016.
[44] H. Bisht, A. Roberts, L. Vogel, A. Bukreyev, P. L. Collins, B. R. Murphy, K. Subbarao, and B. Moss, "Severe acute respiratory syndrome coronavirus spike protein expressed by attenuated vaccinia virus protectively immunizes mice," *Proc. Nat. Acad. Sci. USA*, vol. 101, no. 17, pp. 6641–6646, Apr. 2004, doi: 10.1073/pnas.0401939101.
[45] U. J. Buchholz, A. Bukreyev, L. Yang, E. W. Lamirande, B. R. Murphy, K. Subbarao, and P. L. Collins, "Contributions of the structural proteins of severe acute respiratory syndrome coronavirus to protective immunity," *Proc. Nat. Acad. Sci. USA*, vol. 101, no. 26, pp. 9804–9809, Jun. 2004, doi: 10.1073/pnas.0403492101.
[46] A. Bukreyev, E. W. Lamirande, U. J. Buchholz, and L. N. Vogel, "Mucosal immunisation of African green monkeys (Cercopithecus aethiops) with an attenuated parainfluenza virus expressing the SARS coronavirus spike protein for the prevention of SARS," *Lancet*, vol. 363, no. 9427, pp. 2122–2127, Nov. 2004, doi: 10.1016/S0140-6736(04)16501-X.
[47] R. H. See, A. N. Zakhartchouk, and M. Petric, "Comparative evaluation of two severe acute respiratory syndrome (SARS) vaccine candidates in mice challenged with SARS coronavirus," *J. Gen. Virol.*, vol. 87, no. 3, pp. 641–650, Mar. 2006, doi: 10.1099/vir.0.81579-0.
[48] M. Spruth, O. Kistner, H. Savidis-Dacho, E. Hitter, B. Crowe, M. Gerencer, P. Brühl, L. Grillberger, M. Reiter, C. Tauer, W. Mundt, and P. N. Barrett, "A double-inactivated whole virus candidate SARS coronavirus vaccine stimulates neutralising and protective antibody responses," *Vaccine*, vol. 24, no. 5, pp. 652–661, Jan. 2006, doi: 10.1016/j.vaccine.2005.08.055.
[49] N. Takasuka, "A subcutaneously injected UV-inactivated SARS coronavirus vaccine elicits systemic humoral immunity in mice," *Int. Immunol.*, vol. 16, no. 10, pp. 1423–1430, Aug. 2004, doi: 10.1093/intimm/dxh143.
[50] D. Qu, B. Zheng, X. Yao, Y. Guan, Z.-H. Yuan, N.-S. Zhong, L.-W. Lu, J.-P. Xie, and Y.-M. Wen, "Intranasal immunization with inactivated SARS-CoV (SARS-associated coronavirus) induced local and serum antibodies in mice," *Vaccine*, vol. 23, no. 7, pp. 924–931, Jan. 2005, doi: 10.1016/j.vaccine.2004.07.031.
[51] B. L. P. McKay. (2020). *Drugmakers Rush to Develop Vaccines Against China Virus*. [Online]. Available: https://www.wsj.com/articles/drugmakers-rush-to-develop-vaccines-against-china-virus-11579813026
[52] J. Zhou, W. Wang, Q. Zhong, W. Hou, Z. Yang, and S. Y. Xiao, "Immunogenicity, safety, and protective efficacy of an inactivated SARS-associated coronavirus vaccine in rhesus monkeys," *Vaccine*, vol. 23, no. 24, pp. 3202–3209, Mar. 2005, doi: 10.1016/j.vaccine.2004.11.075.
[53] Xinhua, *China Fast-Tracks Novel Coronavirus Vaccine Development*, Xinhua Net, Beijing, China, 2020.
[54] J. H. Lee, Z. William, and Z. Laura. (2020). *Chinese Scientists Race to Develop Vaccine as Coronavirus Death Toll Jumps*. [Online]. Available: https://www.scmp.com/news/china/society/article/3047676/numbercoronavirus-cases-china-doubles-spread-rate-accelerates
[55] E. Cheung, *China Coronavirus: Hong Kong Researchers Have Already Developed Vaccine But Need Time to Test it, Expert Reveals*, South China Morning Post, Beijing, China, 2020.
[56] Geo-Vax, *Geovax and Bravovax (Wuhan, China) to Collaborate on Development of Coronavirus Vaccine*, Geo-Vax, Atlanta, GA, USA, 2020.
[57] B. Clover, *Clover Initiates Development of Recombinant Subunit-Trimer Vaccine for Wuhan Coronavirus (2019-NCOV): Clover Biopharma*, Clover Biopharmaceuticals, Chengdu, China, 2020.
[58] A. D. Paltiel, A. Zheng, and J. L. Schwartz, "Speed versus efficacy: Quantifying potential tradeoffs in COVID-19 vaccine deployment," *Ann. Internal Med.*, Jan. 2021, doi: 10.7326/M20-7866.
[59] M. D. Knoll and C. Wonodi, "Oxford-AstraZeneca COVID-19 vaccine efficacy," *Lancet*, vol. 397, no. 10269, pp. 72–74, Nov. 2021, doi: 10.1016/S0140-6736(20)32623-4.
[60] NHS, *Novel Coronavirus (COVID-19) Standard Operating Procedure*, NHS England and NHS Improvements, London, U.K., 2020.
[61] M. Gad-el-Hak, *The MEMS Handbook*, vol. 3, Boca Raton, FL, USA: CRC Press, 2005.
[62] C. M. Ho and Y. C. Tai, "Micro-electro-mechanical-systems (MEMS) and fluid flows," *Annu. Rev. Fluid Mech.*, vol. 30, no. 1, pp. 579–612, Jun. 1998, doi: 10.1146/annurev.fluid.30.1.579.
[63] M. J. Madou, "Microfabrication applications," in *Fundamentals Microfabrication*, M. J. Madou, Ed. Boca Raton, FL, USA: CRC Press, 1997, p. 449.
[64] F. Malloggi, "Microfluidics: From basic principles to applications," in *Soft Matter at Aqueous Interfaces*, P. Lang Y. Liu, Eds. Cham, Switzerland: Springer, 2016, pp. 515–546.
[65] D. A. Lamprou, T. R. R. Singh, E. Larrañeta, and R. F. Donnelly, "How innovative drug delivery devices can help realize clinical utility of new effective therapies," *Expert Opinion Drug Del.*, vol. 16, no. 12, pp. 1277–1281, Dec. 2019, doi: 10.1080/17425247.2019.1689956.
[66] E. Callaway, "The race for coronavirus vaccines: A graphical guide," *Nature*, vol. 580, no. 7805, pp. 576–577, Apr. 2020, doi: 10.1038/d41586-020-01221-y.
[67] P. D. Siebert, A. Chenchik, D. E. Kellogg, K. A. Lukyanov, and S. A. Lukyanov, "An improved PCR method for walking in uncloned genomic DNA," *Nucleic Acids Res.*, vol. 23, no. 6, pp. 1087–1088, 1995, doi: 10.1093/nar/23.6.1087.
[68] Perlong Medical Equipment Co. (2020). *Ce Improved PCR Machine Thermal Cycler for DNA Testing Machine High Quality*. [Online]. Available: https://perlong.en.made-in-china.com/product/njaxhkLAOHVv/China-Ce-Improved-PCR-Machine-Thermal-Cycler-for-DNA-Testing-Machine-High-Quality.html
[69] Z. Zhan, C. Dafu, Y. Zhongyao, and W. Li, "Biochip for PCR amplification in silicon," in *Proc. 1st Annu. Int. IEEE-EMBS Special Topic Conf. Microtechnologies Med. Biol.*, Oct. 2000, pp. 25–28.
[70] D. Lee, P.-J. Chen, and G.-B. Lee, "The evolution of real-time PCR machines to real-time PCR chips," *Biosensors Bioelectron.*, vol. 25, no. 7, pp. 1820–1824, Mar. 2010, doi: 10.1016/j.bios.2009.11.021.
[71] Q. Cao, M. Mahalanabis, J. Chang, B. Carey, C. Hsieh, A. Stanley, C. A. Odell, P. Mitchell, J. Feldman, N. R. Pollock, and C. M. Klapperich, "Microfluidic chip for molecular amplification of influenza a RNA in human respiratory specimens," *PLoS ONE*, vol. 7, no. 3, Mar. 2012, Art. no. e33176, doi: 10.1371/journal.pone.0033176.
[72] R. Lu, J. Wang, M. Li, Y. Wang, J. Dong, and W. Cai, "SARS-CoV-2 detection using digital PCR for COVID-19 diagnosis, treatment monitoring and criteria for discharge," *medRxiv*, Mar. 2020, doi: 10.1101/2020.03.24.20042689.
[73] L. Falzone, N. Musso, G. Gattuso, D. Bongiorno, C. Palermo, G. Scalia, M. Libra, and S. Stefani, "Sensitivity assessment of droplet digital PCR for SARS-CoV-2 detection," *Int. J. Mol. Med.*, vol. 46, no. 3, pp. 957–964, Jul. 2020, doi: 10.3892/ijmm.2020.4673.
[74] P. Singru, B. Mistry, R. Shetty, and S. Deopujari, "Design of MEMS based piezo-resistive sensor for measuring pressure in endo-tracheal tube," in *Proc. ASME Int. Mech. Eng. Congr. Expo.*, Houston, TX, USA, Nov. 2015, Art. no. V003T03A036.
[75] ALC. (2020). *Medical Pressure Sensor Applications*. [Online]. Available: https://allsensors.com/applications
[76] D. Träutlein. (2020). *Single-Use Proximal Flow Sensors*. [Online]. Available: https://www.sensirion.com/en/about-us/newsroom/sensirion-specialist-articles/single-use-proximal-flow-sensors/
[77] R. Bogue, "Recent developments in MEMS sensors: A review of applications, markets and technologies," *Sensor Rev.*, vol. 33, no. 4, pp. 300–304, Sep. 2013, doi: 10.1108/sr-05-2013-678.
[78] S. Nihtianov and A. Luque, *Smart Sensors and MEMS: Intelligent Sensing Devices and Microsystems for Industrial Applications*. Cambridge, UK: Woodhead Publishing, 2018.
[79] M. Rajavelu, D. Sivakumar, R. J. Daniel, and K. Sumangala, "Feasibility studies on MEMS oxygen flow sensors by differential pressure method for pediatric ventilators," *J. ISSS*, vol. 1, no. 1, pp. 34–45, Dec. 2012.
[80] S. Silvestri and E. Schena, "Micromachined flow sensors in biomedical applications," *Micromachines*, vol. 3, no. 2, pp. 225–243, Mar. 2012, doi: 10.3390/mi3020225.
[81] B. Tian, H. F. Li, H. Yang, D. L. Song, X. W. Bai, and Y. L. Zhao, "A MEMS SOI-based piezoresistive fluid flow sensor," *Rev. Sci. Instrum.*, vol. 89, no. 2, Feb. 2018, Art. no. 025001, doi: 10.1063/1.5022279.

[82] O. Sazhin and U. Federal University, "Liquid flow meter based on a thermal anemometer microsensor," *J. Appl. Fluid Mech.*, vol. 9, no. 6, pp. 1991–1996, Jul. 2016, doi: 10.18869/acadpub.jafm.68.235.24600.

[83] V. Balakrishnan, T. Dinh, H.-P. Phan, D. V. Dao, and N.-T. Nguyen, "Highly sensitive 3C-SiC on glass based thermal flow sensor realized using MEMS technology," *Sens. Actuators A, Phys.*, vol. 279, pp. 293–305, Aug. 2018, doi: 10.1016/j.sna.2018.06.025.

[84] A. G. P. Kottapalli, M. Asadnia, E. Kanhere, M. S. Triantafyllou, and J. M. Miao, "Smart skin of self-powered hair cell flow sensors for sensing hydrodynamic flow phenomena," in *Proc. 18th Int. Conf. Solid-State Sensors, Actuat. Microsystems (TRANSDUCERS)*, Anchorage, AK, Jun. 2015, pp. 387–390.

[85] Medical Design Briefs. (2020). *Fully Calibrated MEMS-Based Single-Use Proximal Flow Sensors*. [Online]. Available: https://www.medicaldesignbriefs.com/component/content/article/mdb/features/technology-leaders/25748

[86] Electro Pages. (2020). *Ventilator Mass Air Flow Sensors Available in Large Quantities*. [Online]. Available: https://www.electropages.com/2020/04/ventilator-mass-air-flow-sensors-available-large-quantities

[87] A. Alt. (2021). *Flow Sensor Solutions in Modern Medical Ventilators*. [Online]. Available: https://www.sensirion.com/en/about-us/newsroom/sensirion-specialist-articles/flow-sensor-solutions-in-modern-medical-ventilators/

[88] Y. H. Wang, C. P. Chen, C. M. Chang, C. P. Lin, and C. H. Lin, "MEMS-based gas flow sensors," *Microfluidics Nanofluidics*, vol. 6, no. 3, p. 333, Feb. 2009, doi: 10.1007/s10404-008-0383-4.

[89] V. K. Agrawal, R. Patel, D. Boolchandani, and K. Rangra, "Analytical modeling, simulation, and fabrication of a MEMS rectangular paddle piezo-resistive micro-cantilever-based wind speed sensor," *IEEE Sensors J.*, vol. 18, no. 18, pp. 7392–7398, Sep. 2018, doi: 10.1109/JSEN.2018.2860779.

[90] Q. Zhang, W. Ruan, H. Wang, Y. Zhou, Z. Wang, and L. Liu, "A self-bended piezoresistive microcantilever flow sensor for low flow rate measurement," *Sens. Actuators A, Phys.*, vol. 158, no. 2, pp. 273–279, Mar. 2010, doi: 10.1016/j.sna.2010.02.002.

[91] N. Svedin, E. Kalvesten, and G. Stemme, "A new edge-detected lift force flow sensor," *J. Microelectromech. Syst.*, vol. 12, no. 3, pp. 344–354, Jun. 2003, doi: 10.1109/JMEMS.2002.807479.

[92] M. Rajavelu, D. Sivakumar, R. Joseph Daniel, and K. Sumangala, "Perforated diaphragms employed piezoresistive MEMS pressure sensor for sensitivity enhancement in gas flow measurement," *Flow Meas. Instrum.*, vol. 35, pp. 63–75, Mar. 2014, doi: 10.1016/j.flowmeasinst.2013.12.004.

[93] S. Wu, Q. Lin, Y. Yuen, and Y. C. Tai, "MEMS flow sensors for nano-fluidic applications," *Sens. Actuators A, Phys.*, vol. 89, nos. 1–2, pp. 152–158, Feb. 2001, doi: 10.1016/S0924-4247(00)00541-0.

[94] P. Fürjes, G. Légrádi, C. Dücső, A. Aszódi, and I. Bársony, "Thermal characterisation of a direction dependent flow sensor," *Sens. Actuators A, Phys.*, vol. 115, nos. 2–3, pp. 417–423, Sep. 2004, doi: 10.1016/j.sna.2004.04.050.

[95] Z. Tan, M. Shikida, M. Hirota, K. Sato, T. Iwasaki, and Y. Iriye, "Experimental and theoretical study of an on-wall in-tube flexible thermal sensor," *J. Micromech. Microeng.*, vol. 17, no. 4, p. 679, Nov. 2007, doi: 10.1088/0960-1317/17/4/002.

[96] E. Meng, P.-Y. Li, and Y.-C. Tai, "A biocompatible parylene thermal flow sensing array," *Sens. Actuators A, Phys.*, vol. 144, no. 1, pp. 18–28, May 2008, doi: 10.1016/j.sna.2007.12.010.

[97] S. Dalola, S. Cerimovic, F. Kohl, R. Beigelbeck, J. Schalko, V. Ferrari, D. Marioli, F. Keplinger, and T. Sauter, "MEMS thermal flow sensor with smart electronic interface circuit," *IEEE Sensors J.*, vol. 12, no. 12, pp. 3318–3328, Dec. 2012, doi: 10.1109/JSEN.2012.2219619.

[98] R. G. Johnson and R. E. Higashi, "A highly sensitive silicon chip microtransducer for air flow and differential pressure sensing applications," *Sens. Actuators*, vol. 11, no. 1, pp. 63–72, Jun. 1987, doi: 10.1016/0250-6874(87)85005-9.

[99] T. S. J. Lammerink, N. R. Tas, M. Elwenspoek, and J. H. J. Fluitman, "Micro-liquid flow sensor," *Sens. Actuators A, Phys.*, vol. 37, pp. 45–50, Nov. 1993, doi: 10.1016/0924-4247(93)80010-E.

[100] F. Kohl, A. Jachimowicz, J. Steurer, and R. Glatz, "A micromachined flow sensor for liquid and gaseous fluids," *Sens. Actuators A, Phys.*, vol. 41, nos. 1–3, pp. 293–299, Nov. 1994, doi: 10.1016/0924-4247(94)80126-6.

[101] F. Mailly, A. Giani, R. Bonnot, and P. Temple-Boyer, "Anemometer with hot platinum thin film," *Sens. Actuators A, Phys.*, vol. 94, nos. 1–2, pp. 32–38, Jan. 2001, doi: 10.1016/S0924-4247(01)00668-9.

[102] J. J. Van Baar, R. J. Wiegerink, T. S. J. Lammerink, G. J. M. Krijnen, and M. Elwenspoek, "Micromachined structures for thermal measurements of fluid and flow parameters," *J. Micromech. Microeng.*, vol. 11, no. 4, p. 311, Feb. 2001, doi: 10.1088/0960-1317/11/4/304.

[103] N. Svedin, E. Kälvesten, and G. Stemme, "A lift force sensor with integrated hot-chips for wide range flow measurements," *Sens. Actuators A, Phys.*, vol. 109, nos. 1–2, pp. 120–130, Dec. 2003, doi: 10.1016/j.sna.2003.05.003.

[104] M. Dijkstra, M. J. de Boer, J. W. Berenschot, T. S. J. Lammerink, R. J. Wiegerink, and M. Elwenspoek, "Miniaturized thermal flow sensor with planar-integrated sensor structures on semicircular surface channels," *Sens. Actuators A, Phys.*, vol. 143, no. 1, pp. 1–6, May 2008, doi: 10.1016/j.sna.2007.12.005.

[105] C.-H. Wu, D. Kang, P.-H. Chen, and Y.-C. Tai, "MEMS thermal flow sensors," *Sens. Actuators A, Phys.*, vol. 241, pp. 135–144, Apr. 2016, doi: 10.1016/j.sna.2016.02.018.

[106] Y. Su, A. G. R. Evans, and A. Brunnschweiler, "Micromachined silicon cantilever paddles with piezoresistive readout for flow sensing," *J. Micromech. Microeng.*, vol. 6, no. 1, p. 69, Nov. 1996, doi: 10.1088/0960-1317/6/1/015.

[107] N. Svedin, E. Stemme, and G. Stemme, "A new bi-directional gas-flow sensor based on lift force," in *Proc. Int. Solid State Sens. Actuators Conf. (Transducers)*, Chicago, IL, USA, 1997, pp. 145–148.

[108] Y. Su, A. Evans, A. Brunnschweiler, and G. Ensell, "Characterization of a highly sensitive ultra-thin piezoresistive silicon cantilever probe and its application in gas flow velocity sensing," *J. Micromech. Microeng.*, vol. 12, no. 6, p. 780, Nov. 2002, doi: 10.1088/0960-1317/12/6/309.

[109] Y.-H. Wang, C.-Y. Lee, and C.-M. Chiang, "A MEMS-based air flow sensor with a free-standing micro-cantilever structure," *Sensors*, vol. 7, no. 10, pp. 2389–2401, Oct. 2007, doi: 10.3390/s7102389.

[110] A. K. Dhonkal, V. Agarwal, and K. Sengar, "Sensitivity of the MEMS based piezoresistive wind speed sensor with comparative study of different shapes of paddles," *Int. Res. J. Eng. Technol.*, vol. 4, no. 2, pp. 1693–1697, Feb. 2017.

[111] P. Bruschi, M. Dei, and M. Piotto, "A low-power 2-D wind sensor based on integrated flow meters," *IEEE Sensors J.*, vol. 9, no. 12, pp. 1688–1696, Dec. 2009, doi: 10.1109/JSEN.2009.2030652.

[112] A. S. Cubukcu, E. Zernickel, U. Buerklin, and G. A. Urban, "A 2D thermal flow sensor with sub-mW power consumption," *Sens. Actuators A, Phys.*, vol. 163, no. 2, pp. 449–456, Oct. 2010, doi: 10.1016/j.sna.2010.08.012.

[113] Y. Ye, Z. Yi, S. Gao, M. Qin, and Q.-A. Huang, "DRIE trenches and full-bridges for improving sensitivity of 2-D micromachined silicon thermal wind sensor," *J. Microelectromech. Syst.*, vol. 26, no. 5, pp. 1073–1081, Oct. 2017, doi: 10.1109/JMEMS.2017.2707558.

[114] Z. Li, W. Chang, C. Gao, and Y. Hao, "A novel five-wire micro anemometer with 3D directionality for low speed air flow detection and acoustic particle velocity detecting capability," *J. Micromech. Microeng.*, vol. 28, no. 4, Apr. 2018, Art. no. 044004, doi: 10.1088/1361-6439/aaac63.

[115] W. Xu, B. Gao, S. Ma, A. Zhang, Y. Chiu, and Y. K. Lee, "Low-cost temperature-compensated thermoresistive micro calorimetric flow sensor by using 0.35 μm CMOS MEMS technology," in *Proc. IEEE 29th Int. Conf. Micro Electro Mech. Syst. (MEMS)*, Shanghai, China, Jan. 2016, pp. 189–192.

[116] N. Sabaté, J. Santander, L. Fonseca, I. Gràcia, and C. Cané, "Multi-range silicon micromachined flow sensor," *Sens. Actuators A, Phys.*, vol. 110, nos. 1–3, pp. 282–288, Feb. 2004, doi: 10.1016/j.sna.2003.10.068.

[117] E. Meng and Y.-C. Tai, "A parylene MEMS flow sensing array," in *Proc. 12th Int. Conf. Solid-State Sensors, Actuat. Microsystems. Dig. Tech. Papers (TRANSDUCERS)*, Boston, MA, USA, Jun. 2003, pp. 686–689.

[118] C. Hoera, M. M. Skadell, S. A. Pfeiffer, M. Pahl, Z. Shu, E. Beckert, and D. Belder, "A chip-integrated highly variable thermal flow rate sensor," *Sens. Actuators B, Chem.*, vol. 225, pp. 42–49, Mar. 2016, doi: 10.1016/j.snb.2015.11.009.

[119] M. Shikida, T. Matsuyama, T. Yamada, M. Matsushima, and T. Kawabe, "Development of implantable catheter flow sensor into inside of bronchi for laboratory animal," *Microsyst. Technol.*, vol. 23, no. 1, pp. 175–185, Jan. 2017, doi: 10.1007/s00542-015-2663-8.

[120] H. Yoshida, Y. Hasegawa, M. Matsushima, T. Sugiyama, T. Kawabe, and M. Shikida, "Micro-machined respiratory monitoring system development for artificial ventilator in animal experiment," *Microsyst. Technol.*, vol. 26, no. 12, pp. 3715–3724, Dec. 2020, doi: 10.1007/s00542-020-04844-3.

[121] H. Devaraj, R. Sharma, E. Haemmerle, and K. Aw, "A portable & disposable ultra-low velocity flow sensor from bioinspired hair-like microstructures," *Proceedings*, vol. 2, no. 13, p. 731, Dec. 2018.
[122] W. Ke, M. Liu, T. Li, and Y. Wang, "MEMS thermal gas flow sensor with self-test function," *J. Micromech. Microeng.*, vol. 29, no. 12, Dec. 2019, Art. no. 125009, doi: 10.1088/1361-6439/ab4aef.
[123] A. G. P. Kottapalli, Z. Shen, M. Asadnia, S. Tian, K. Tao, J. Miao, and M. S. Triantafyllou, "Polymer MEMS sensor for flow monitoring in biomedical device applications," in *Proc. IEEE 30th Int. Conf. Micro Electro Mech. Syst. (MEMS)*, Las Vegas, NV, USA, Jan. 2017, pp. 632–635.
[124] G. Zhou, Y. Zhao, F. Guo, and W. Xu, "A smart high accuracy silicon piezoresistive pressure sensor temperature compensation system," *Sensors*, vol. 14, no. 7, pp. 12174–12190, Jul. 2014, doi: 10.3390/s140712174.
[125] S. Hiremath and S. M. Kulkarni, "Modelling and analysis of polymer diaphragms for micro sensing and actuation," in *Proc. AIP Conf.*, Jan. 2019, vol. 2080, no. 1, Art. no. 020004, doi: 10.1063/1.5092887.
[126] F. Ejeian, S. Azadi, A. Razmjou, Y. Orooji, A. Kottapalli, M. Ebrahimi Warkiani, and M. Asadnia, "Design and applications of MEMS flow sensors: A review," *Sens. Actuators A, Phys.*, vol. 295, pp. 483–502, Aug. 2019, doi: 10.1016/j.sna.2019.06.020.
[127] M. Bora, A. G. P. Kottapalli, J. M. Miao, and M. S. Triantafyllou, "Fish-inspired self-powered microelectromechanical flow sensor with biomimetic hydrogel cupula," *APL Mater.*, vol. 5, no. 10, Oct. 2017, Art. no. 104902, doi: 10.1063/1.5009128.
[128] S. C. P. Kumar and D. Jyothsna, "Biomedical applications of Mems & Nems pressure transducers/sensors," *Int. J. Innov. Res. Develop.*, vol. 2, p. 5, Dec. 2013.
[129] M. A. Matthay, J. M. Aldrich, and J. E. Gotts, "Treatment for severe acute respiratory distress syndrome from COVID-19," *Lancet Respiratory Med.*, vol. 8, no. 5, pp. 433–434, May 2020, doi: 10.1016/s2213-2600(20)30127-2.
[130] M. Kaisti, J Leppänen, and O. Lahdenoja, "Wearable pressure sensor array for health monitoring," in *Proc. Comput. Cardiol. (CinC)*, Rennes, France, Jul. 2017, pp. 1–4.
[131] J. Miguel, Y. Lechuga, and M. Martinez, "AFM-based characterization method of capacitive MEMS pressure sensors for cardiological applications," *Micromachines*, vol. 9, no. 7, p. 342, Jul. 2018, doi: 10.3390/mi9070342.
[132] A. D. Sundararajan, "High sensitive absolute MEMS capacitive pressure sensor in SiGeMEMS process for biomedical applications," *Int. J. Civil Eng. Technol.*, vol. 8, no. 9, pp. 512–519, Nov. 2017.
[133] K. Kashish, M. Priya, and P. Yadav, "Design of low power pulse oximeter for early detection of hypoxemia," in *Proc. Int. Conf. Micro-Electron. Telecommun. Eng. (ICMETE)*, Sep. 2016, pp. 600–605.
[134] L. Gattinoni, D. Chiumello, P. Caironi, M. Busana, F. Romitti, L. Brazzi, and L. Camporota, "COVID-19 pneumonia: Different respiratory treatments for different phenotypes?" *Intensive Care Med.*, vol. 46, no. 6, pp. 1099–1102, Jun. 2020, doi: 10.1007/s00134-020-06033-2.
[135] World Health Organization, *Handbook: IMCI Integrated Management of Childhood Illness*, WHO, Geneva, Switzerland, 2005.
[136] V. Alwadhi, P. Dewan, R. K. Malhotra, D. Shah, and P. Gupta, "Tachypnea and other danger signs vs pulse oximetry for prediction of hypoxia in severe pneumonia/very severe disease," *Indian Pediatrics*, vol. 54, no. 9, pp. 729–734, Sep. 2017, doi: 10.1007/s13312-017-1163-6.
[137] S. Basnet, R. K. Adhikari, and C. K. Gurung, "Hypoxemia in children with pneumonia and its clinical predictors," *Indian J. Pediatrics*, vol. 73, no. 9, pp. 777–781, Sep. 2006, doi: 10.1007/BF02790384.
[138] T. Duke, R. Subhi, D. Peel, and B. Frey, "Pulse oximetry: Technology to reduce child mortality in developing countries," *Ann. Tropical Paediatrics*, vol. 29, no. 3, pp. 165–175, Sep. 2009, doi: 10.1179/027249309X12467994190011.
[139] E. D. McCollum, E. Bjornstad, G. A. Preidis, M. C. Hosseinipour, and N. Lufesi, "Multicenter study of hypoxemia prevalence and quality of oxygen treatment for hospitalized malawian children," *Trans. Roy. Soc. Tropical Med. Hygiene*, vol. 107, no. 5, pp. 285–292, May 2013, doi: 10.1093/trstmh/trt017.
[140] S. Sazawal, R. E. Black, and P. C. M. T. Group, "Effect of pneumonia case management on mortality in neonates, infants, and preschool children: A meta-analysis of community-based trials," *Lancet Infectious Diseases*, vol. 3, no. 9, pp. 547–556, Dec. 2003, doi: 10.1016/S1473-3099(03)00737-0.
[141] O. T. Uwemedimo, T. P. Lewis, E. A. Essien, G. J. Chan, H. Nsona, M. E. Kruk, and H. H. Leslie, "Distribution and determinants of pneumonia diagnosis using integrated management of childhood illness guidelines: A nationally representative study in malawi," *BMJ Global Health*, vol. 3, no. 2, Mar. 2018, Art. no. e000506, doi: 10.1136/bmjgh-2017-000506.
[142] E. D. McCollum and A. S. Ginsburg, "Outpatient management of children with world health organization chest indrawing pneumonia: Implementation risks and proposed solutions," *Clin. Infectious Diseases*, vol. 65, no. 9, pp. 1560–1564, Oct. 2017, doi: 10.1093/cid/cix543.
[143] P.-J. Chen, D. C. Rodger, S. Saati, M. S. Humayun, and Y.-C. Tai, "Implantable parylene-based wireless intraocular pressure sensor," in *Proc. IEEE 21st Int. Conf. Micro Electro Mech. Syst.*, Tucson, AZ, USAJan. 2008, pp. 58–61.
[144] P. Bingger, J. Fiala, A. Seifert, N. Weber, K. Foerster, C. Heilmann, F. Beyersdorf, P. Woias, and H. Zappe, "*in vivo* monitoring of blood oxygenation using an implantable MEMS-based sensor," in *Proc. IEEE 23rd Int. Conf. Micro Electro Mech. Syst. (MEMS)*, Hong Kong, Jan. 2010, pp. 1031–1034.
[145] D. She, "The development of MEMS-based implantable oxygen sensing systems," Ph.D. dissertation, Electr. Syst. Eng., Univ. Pennsylvania, Philadelphia, PA, USA, 2019.
[146] Y. Oh, Y.-J. Jung, S. Choi, and D. Kim, "Design and evaluation of a MEMS magnetic field sensor-based respiratory monitoring and training system for radiotherapy," *Sensors*, vol. 18, no. 9, p. 2742, Aug. 2018, doi: 10.3390/s18092742.
[147] T.-V. Nguyen, Y. Mizuki, T. Tsukagoshi, T. Takahata, M. Ichiki, and I. Shimoyama, "MEMS-based pulse wave sensor utilizing a piezoresistive cantilever," *Sensors*, vol. 20, no. 4, p. 1052, Feb. 2020, doi: 10.3390/s20041052.
[148] T.-V. Nguyen and M. Ichiki, "Simultaneous measurement of pulse wave and respiration using a single tube-shaped MEMS-based pressure sensor," in *Proc. IEEE 33rd Int. Conf. Micro Electro Mech. Syst. (MEMS)*, Vancouver, BC, Canada, Jan. 2020, pp. 84–87.
[149] GIMA. (2021). *Auto Syringe Pump*. [Online]. Available: https://www.gimaitaly.com/prodotti.asp?sku=35205&dept_selected=62&dept_id=628
[150] R. A. Snijder, T. C. G. Egberts, P. Lucas, P. M. A. Lemmers, F. van Bel, and A. M. D. E. Timmerman, "Dosing errors in preterm neonates due to flow rate variability in multi-infusion syringe pump setups: An in vitro spectrophotometry study," *Eur. J. Pharmaceutical Sci.*, vol. 93, pp. 56–63, Oct. 2016, doi: 10.1016/j.ejps.2016.07.019.
[151] H. Well, "Sensors in infusion pumps," Honeywell International Inc., Charlotte, NC, USA, Honeywell Sensor Appl. Notes 008045-9-EN, 2020.
[152] X. Ma, P. Guo, X. Tong, Y. Zhao, Q. Zhang, P. Ke, and A. Wang, "Piezoresistive behavior of amorphous carbon films for high performance MEMS force sensors," *Appl. Phys. Lett.*, vol. 114, no. 25, Jun. 2019, Art. no. 253502, doi: 10.1063/1.5096225.
[153] M. Lamba, N. Mittal, K. Singh, and H. Chaudhary, "Design analysis of polysilicon piezoresistors PDMS (Polydimethylsiloxane) microcantilever based MEMS force sensor," *Int. J. Mod. Phys. B*, vol. 34, no. 09, Apr. 2020, Art. no. 2050072, doi: 10.1142/S0217979220500721.
[154] B. Liang, W. Chen, Z. He, R. Yang, Z. Lin, H. Du, Y. Shang, A. Cao, Z. Tang, and X. Gui, "Highly sensitive, flexible MEMS based pressure sensor with photoresist insulation layer," *Small*, vol. 13, no. 44, Nov. 2017, Art. no. 1702422, doi: 10.1002/smll.201702422.
[155] M. Nag, J. Singh, A. Kumar, P. A. Alvi, and K. Singh, "Sensitivity enhancement and temperature compatibility of graphene piezoresistive MEMS pressure sensor," *Microsyst. Technol.*, vol. 25, no. 10, pp. 3977–3982, Oct. 2019, doi: 10.1007/s00542-019-04392-5.
[156] L. S. Panwar, S. Kala, V. Panwar, S. S. Panwar, and S. Sharma, "Design of MEMS piezoelectric blood pressure sensor," in *Proc. 3rd Int. Conf. Adv. Computing, Commun. Autom. (ICACCA) (Fall)*, Dehradun, India, Sep. 2017, pp. 1–7.
[157] K. S. Rao, W. Samyuktha, D. V. Vardhan, B. G. Naidu, P. A. Kumar, K. G. Sravani, and K. Guha, "Design and sensitivity analysis of capacitive MEMS pressure sensor for blood pressure measurement," *Microsyst. Technol.*, vol. 26, no. 8, pp. 2371–2379, Aug. 2020, doi: 10.1007/s00542-020-04777-x.
[158] P. Song, C. Si, M. Zhang, Y. Zhao, Y. He, W. Liu, and X. Wang, "A novel piezoresistive MEMS pressure sensors based on temporary bonding technology," *Sensors*, vol. 20, no. 2, p. 337, Jan. 2020, doi: 10.3390/s20020337.

[159] C. Y. Lin and K. A. Wen, "MEMS resonator based thermometer SoC design in CMOS 0.18 μm standard process," in *Proc. Int. SoC Design Conf. (ISOCC)*, Jeju, South Korea, Oct. 2016, pp. 13–14.
[160] C.-W. Hsu and K.-A. Wen, "Monolithic integration of digital MEMS thermometer and temperature compensated RTC on 1P6M ASIC compatible CMOS MEMS process," in *Proc. IEEE Int. Conf. Semiconductor Electron. (ICSE)*, Kuala Lumpur, Malaysia, Aug. 2018, pp. 45–48.
[161] S. Xiao, L. Che, X. Li, and Y. Wang, "A cost-effective flexible MEMS technique for temperature sensing," *Microelectron. J.*, vol. 38, no. 3, pp. 360–364, Mar. 2007, doi: 10.1016/j.mejo.2007.01.022.
[162] L. M. Yu, F. E. H. Tay, D. G. Guo, L. Xu, M. N. Nyan, F. W. Chong, K. L. Yap, and B. Xu, "A MEMS-based bioelectrode for ECG measurement," in *Proc. IEEE Sensors*, Lecce, Italy, Oct. 2008, pp. 1068–1071.
[163] H.-L. Kim, Y.-H. Kim, and Y.-J. Kim, "Miniature electrocardiography sensor using a flexible printed circuit and MEMS technology," in *Proc. IEEE Int. Conf. Multisensor Fusion Integr. Intell. Syst.*, Seoul, South Korea, Aug. 2008, pp. 545–550.
[164] A. Usman, M. Mukhtar, and R. M. Umer, "MEMS based wireless energy harvesting mechanism for ECG and BCG application," in *Proc. Int. Conf. Emerg. Technol. (ICET)*, Islamabad, Pakistan, Dec. 2014, pp. 142–146.
[165] J. E. Hernandez and E. Cretu, "Simple heart rate monitoring system with a MEMS gyroscope for sleep studies," in *Proc. IEEE 9th Annu. Inf. Technol., Electron. Mobile Commun. Conf. (IEMCON)*, Vancouver, BC, Canada, Nov. 2018, pp. 61–67.
[166] W. Wang, Q. Xu, G. Zhang, Y. Lian, L. Zhang, X. Zhang, Y. Shi, S. Duan, and R. Wang, "A bat-shape piezoresistor electronic stethoscope based on MEMS technology," *Measurement*, vol. 147, Dec. 2019, Art. no. 106850, doi: 10.1016/j.measurement.2019.106850.
[167] G. Zhang, M. Liu, N. Guo, and W. Zhang, "Design of the MEMS piezoresistive electronic heart sound sensor," *Sensors*, vol. 16, no. 11, p. 1728, Nov. 2016, doi: 10.3390/s16111728.
[168] D. N. Mathias, J. Park, E. Kim, and Y.-H. Joung, "Development of a novel noncontact ECG electrode by MEMS fabrication process," *Trans. Electr. Electron. Mater.*, vol. 17, no. 3, pp. 150–154, Jun. 2016, doi: 10.4313/TEEM.2016.17.3.150.
[169] S. Meti, K. B. Balavald, and B. Sheeparmatti, "MEMS piezoresistive pressure sensor: A survey," *Int. J. Eng. Res. Appl.*, vol. 6, no. 4, pp. 23–31, Jan. 2016.
[170] A. Hedayatipour and N. Mcfarlane, "Wearables for the next pandemic," *IEEE Access*, vol. 8, pp. 184457–184474, Sep. 2020, doi: 10.1109/ACCESS.2020.3029130.
[171] F. Ali, W. Raza, X. Li, H. Gul, and K.-H. Kim, "Piezoelectric energy harvesters for biomedical applications," *Nano Energy*, vol. 57, pp. 879–902, Mar. 2019, doi: 10.1016/j.nanoen.2019.01.012.
[172] M. T. Todaro, F. Guido, V. Mastronardi, D. Desmaele, G. Epifani, L. Algieri, and M. De Vittorio, "Piezoelectric MEMS vibrational energy harvesters: Advances and outlook," *Microelectron. Eng.*, vols. 183–184, pp. 23–36, Nov. 2017, doi: 10.1016/j.mee.2017.10.005.
[173] D. Zhou, N. Wang, T. Yang, L. Wang, X. Cao, and Z. L. Wang, "A piezoelectric nanogenerator promotes highly stretchable and self-chargeable supercapacitors," *Mater. Horizons*, vol. 7, no. 8, pp. 2158–2167, Aug. 2020, doi: 10.1039/D0MH00610F.
[174] C. Chen, Z. Bai, Y. Cao, M. Dong, K. Jiang, Y. Zhou, Y. Tao, S. Gu, J. Xu, X. Yin, and W. Xu, "Enhanced piezoelectric performance of $BiCl_3$/PVDF nanofibers-based nanogenerators," *Composites Sci. Technol.*, vol. 192, May 2020, Art. no. 108100, doi: 10.1016/j.compscitech.2020.108100.

MUHAMMAD SHAHBAZ KHAN received the B.S. degree in electronics engineering from the NFC Institute of Engineering and Technology, Multan, Pakistan, in 2011, and the M.S. degree in electrical engineering from HITEC University, Taxila, Pakistan, in 2015. He is currently pursuing the Ph.D. degree in electrical engineering with Riphah International University, Islamabad, Pakistan. He is also a Lecturer with the Department of Electrical Engineering, HITEC University. His research interests include MEMS sensors and actuators, Bio-MEMS, and microfabrication.

MUHAMMAD OWAIS TARIQ received the B.Sc. degree in electronics engineering from the NFC Institute of Engineering and Technology, Multan, Pakistan, in 2011, and the M.S. degree in electrical engineering from the College of Electrical and Mechanical Engineering (CEME), NUST, Islamabad, Pakistan. He is currently pursuing the Ph.D. degree in electrical engineering with Riphah International University, Islamabad. He is also working as an Assistant Professor with the Pakistan Institute of Engineering and Technology, Multan. His research interest includes microelectromechanical device designing for biomedical and pharmaceutical applications.

MENAA NAWAZ received the B.S. degree in electronics engineering from the NFC Institute of Engineering and Technology, Multan, Pakistan, in 2009, and the M.S. degree in electrical engineering from HITEC University, Taxila, Pakistan, in 2014. She is currently pursuing the Ph.D. degree in electrical engineering with Riphah International University, Islamabad. Since 2013, she has been working as an Assistant Professor with HITEC University. Her research interests include wireless sensor networks, design, and analysis of IoT-based healthcare systems, and time series analysis of physiological signals.

JAMEEL AHMED (Member, IEEE) received the B.S. degree in electronic engineering from the NED University of Engineering and Technology, Karachi, the M.S. degree in electrical engineering from the National University of Sciences and Technology (NUST), Pakistan, and the Ph.D. degree in communication engineering from Pakistan and Nanyang Technological University (NTU), Singapore. He also received two Postdoctorate Fellowships from the School of Electrical and Electronic Engineering (EEE), NTU. He is currently a Professor and the Dean of the Faculty of Engineering and Applied Sciences, Riphah International University, Islamabad, Pakistan. He has 27 years of professional experience in undergraduate and graduate-level teaching, research and management. He has published more than 50 research publications at the National and international level and also authored/coauthored eight books/handbook including three by Springer-Verlag. He is a member of IEEE-USA and its three societies. He is also an elected member of Board of Governors (BoG), Engineering Accreditation Board (EAB), and Engineering Curriculum Review & Development Committee (ECRDC) of Pakistan Engineering Council (PEC).